# Direct and indirect $\alpha$ transfer in the elastic $^{16}$O+$^{12}$C scattering

Nguyen Tri Toan Phuc[1,2], Nguyen Hoang Phuc[1], and Dao T. Khoa[1]

[1] *Institute for Nuclear Science and Technology, VINATOM*

*179 Hoang Quoc Viet, Cau Giay, Hanoi, Vietnam.*

[2] *VNUHCM-University of Science, Ho Chi Minh City, Vietnam*

(Dated: August 3, 2018)

## Abstract

The extensive elastic $^{16}$O+$^{12}$C scattering data measured at low energies show consistently an oscillating enhancement of the elastic cross section at backward angles that is difficult to describe within the conventional optical model. Given the significant $\alpha$ spectroscopic factors predicted for the dissociation $^{16}$O$\rightarrow \alpha+^{12}$C by the shell model (SM) and $\alpha$-cluster model calculations, the contribution of the $\alpha$ transfer channels to the elastic $^{16}$O+$^{12}$C scattering should not be negligible, and is expected to account for the enhanced oscillation of the elastic cross section at backward angles. To reveal the impact of the $\alpha$ transfer, a systematic coupled reaction channels (CRC) analysis of the elastic $^{16}$O+$^{12}$C scattering has been performed where the multistep couplings between the elastic and inelastic scattering channels, the direct and indirect $\alpha$ transfer channels were treated explicitly, using the real optical potentials and inelastic scattering form factors determined by the double-folding model. We show that a consistent CRC description of the elastic $^{16}$O+$^{12}$C data at different energies can be obtained over the whole angular region, using the $\alpha$ spectroscopic factors determined recently in the large scale SM calculation. The present CRC results are, therefore, of interest not only for the nuclear scattering studies but also provide an important spectroscopic information on the cluster dissociation of $^{16}$O.

# I. INTRODUCTION

While the elastic heavy-ion (HI) scattering is usually dominated by the strong absorption [1, 2], some light HI systems are weak absorbing and refractive enough for the appearance of the nuclear rainbow pattern at medium and large angles, which allows the determination of the real nucleus-nucleus optical potential (OP) with a much less ambiguity (see, e.g., the topical review [3] for more detail). As discussed in a recent folding model analysis [4] of the elastic $^{12}$C+$^{12}$C and $^{16}$O+$^{12}$C scattering, there is a range of the refractive energies ($10 \lesssim E \lesssim 40$ MeV/nucleon for the incident $^{12}$C and $^{16}$O ions), where the nuclear rainbow pattern can be clearly observed. Although the $^{12}$C+$^{12}$C and $^{16}$O+$^{16}$O systems are strongly refractive, the rainbow pattern cannot be observed at $\theta_{\text{c.m.}} > 90°$ because of the boson symmetry of the two identical nuclei that leads to a rapidly oscillating elastic cross section around the angle $\theta_{\text{c.m.}} = 90°$. The $^{16}$O+$^{12}$C system does not have the boson symmetry and was considered as a good candidate for the study of the nuclear rainbow [5]. For that purpose, several experiments have been performed to measure the elastic $^{16}$O+$^{12}$C scattering with high-precision, covering a wide range of energies ($E_{\text{lab}} \approx 20 - 1503$ MeV) and a broad angular region (up to $\theta_{\text{c.m.}} > 130°$ at low energies) [6–12]. Very interesting are the elastic $^{16}$O+$^{12}$C data measured at the HI cyclotrons of the Kurchatov institute and university of Jyväskylä [9, 10], which were shown to exhibit a pronounced nuclear rainbow pattern [4, 10], and the low-energy data measured at the Strasbourg Tandem Vivitron [11]. The extensive optical model (OM) and folding model studies of the elastic $^{16}$O+$^{12}$C scattering [4, 13–18] have shown unambiguously the nuclear rainbow pattern in this system. However, at low energies ($E_{\text{lab}} \lesssim 132$ MeV) the smooth rainbow pattern at backward angles is strongly deteriorated by a quick oscillation of the elastic $^{16}$O+$^{12}$C cross section (see, e.g., the upper panel of Fig. 11 in Ref. [4]). In the conventional OM using the empirical Woods-Saxon (WS) potentials, one could obtain a good description of the low-energy elastic $^{16}$O+$^{12}$C data only if an extremely small diffuseness ($a_V \lesssim 0.1$ fm) of the absorptive WS potential is used [11]. Such an abrupt shape of the absorptive WS potential is drastically different from the global systematics of the complex OP for the $^{16}$O+$^{12}$C system [2].

In the present study, we focus on the high-precision elastic $^{16}$O+$^{12}$C scattering data, measured at low energies of 5 to 8 MeV/nucleon [9–11], over the center-of-mass (c.m.) angles up to around 170°. Note that the OM analyses of the elastic $^{16}$O+$^{12}$C data available

2
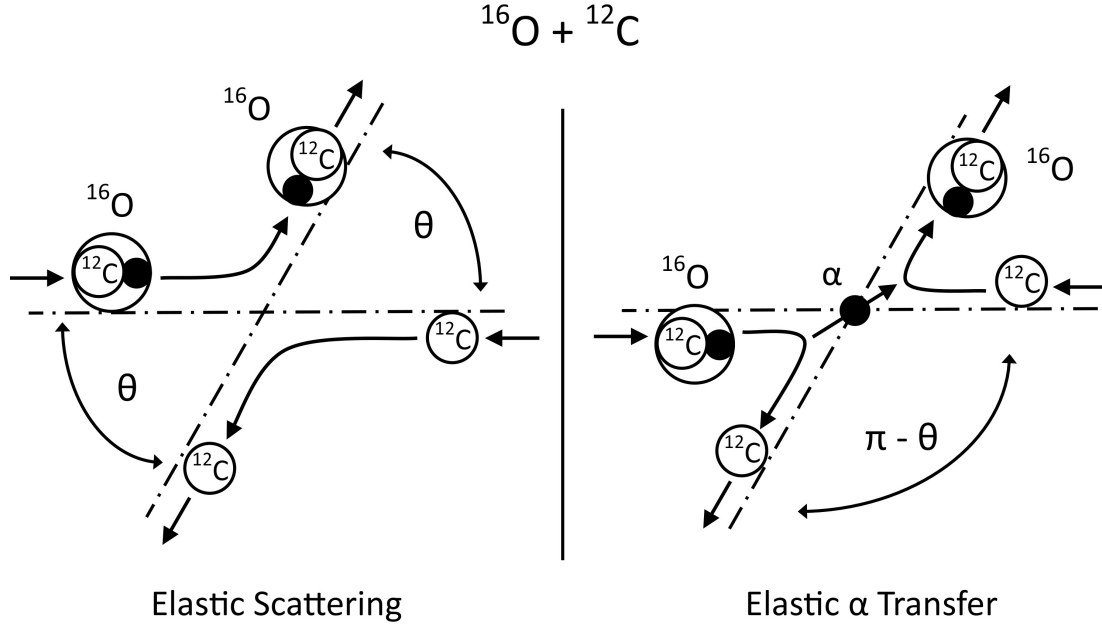
FIG. 1. Kinematical illustration of the elastic scattering and elastic $\alpha$ transfer processes in the $^{16}$O+$^{12}$C system.

in the seventies and early eighties faced about the same problem [19, 20], and a parity-dependent term was often added to the complex OP which was suggested by von Oertzen and Bohlen [20] as necessary to effectively account for the core exchange symmetry or the elastic $\alpha$ transfer between $^{16}$O and $^{12}$C (see Fig. 1). Guided by such a scenario, Szilner $et$ $al.$ [21] have analyzed the Strasbourg data measured at $E_{\text{lab}} = 100$, 115.9, and 124 MeV [11] within the coupled reaction channels (CRC) approach, explicitly taking into account the coupling between the elastic scattering and direct (elastic) $\alpha$ transfer channels. The observed oscillating cross sections at large angles were well described by these CRC results [21], where the WS forms were used for the real OP and a weakly absorptive imaginary OP having "standard" diffuseness of around $0.5 - 0.6$ fm. Similar analyses of the direct $\alpha$ transfer in the elastic $^{16}$O+$^{12}$C scattering at energies near the Coulomb barrier were done in the distorted wave Born approximation (DWBA) [22, 23]. In these studies, parameters of the OP were fitted to the best OM description of the elastic cross section at forward angles, and the overall good description of the elastic $^{16}$O+$^{12}$C data was achieved with a DWBA amplitude of the direct $\alpha$ transfer added to the elastic scattering amplitude. The different elastic transfer processes in the elastic $^{16}$O+$^{12}$C scattering at low energies were

studied in the CRC calculation by Rudchik *et al.* [24], and they were shown to contribute significantly to the elastic cross section. These CRC results show, however, a very weak contribution from the $\alpha$ transfer to the elastic cross section at backward angles. At variance with the conclusions made in the studies mentioned above, Ohkubo and Hirabayashi [25] have proposed a completely different scenario for the quickly oscillating elastic $^{16}$O+$^{12}$C cross section at backward angles based on the results of their coupled channel (CC) analysis of the elastic $^{16}$O+$^{12}$C data measured at $E_{\text{lab}} = 115.9$ MeV. Namely, the oscillatory pattern at large angles was interpreted as the nuclear "ripples" given by an interference between the elastic scattering wave and the external reflective wave (caused by the nuclear excitations taken into account in the CC calculation). Thus, the true physics origin of the oscillating enhancement of the elastic $^{16}$O+$^{12}$C cross section at backward angles, observed at energies $E_{\text{lab}} \lesssim 132$ MeV, is still under discussion.

To explore the impact of the $\alpha$ transfer on the elastic $^{16}$O+$^{12}$C scattering, we have performed in the present work a systematic CRC analysis of the low-energy elastic $^{16}$O+$^{12}$C scattering data measured at the energies $E_{\text{lab}} = 100 - 124$ MeV by Strasbourg group [11], the data measured at $E_{\text{lab}} = 132$ MeV by Kurchatov group [9, 10], and the interesting data measured at $E_{\text{lab}} = 300$ MeV by Brandan *et al.* [12] including the data points at the most backward angles that could not be described so far in the standard OM analysis. A proper choice of the OP for both the $^{16}$O+$^{12}$C and $^{12}$C+$^{12}$C systems is vital for the CRC analysis of the elastic $^{16}$O+$^{12}$C scattering at low energies. The real OP for these systems at the refractive energies has been shown to be well described by the (mean-field based) double-folded potential [4]. In a smooth continuation to lower energies, the recently extended version of the double-folding model (DFM) [4] is used throughout the present work to evaluate the real OP for the $^{12}$C+$^{12}$C and $^{16}$O+$^{12}$C systems. The imaginary OP is chosen in the phenomenological WS form, with parameters taken from the global systematics [2] of the elastic light HI scattering. These WS parameters are further fine-tuned to accurately reproduce the diffraction of the elastic $^{16}$O+$^{12}$C cross section at forward angles that is determined overwhelmingly by the true elastic scattering. In this way, a proper CRC description of the oscillatory structure in the elastic $^{16}$O+$^{12}$C cross section at backward angles should allow us to properly assess the contribution from the $\alpha$ transfer process to the elastic $^{16}$O+$^{12}$C scattering.

In the first order of the CRC formalism, the coupling between the elastic scattering $^{12}$C

($^{16}$O,$^{16}$O)$^{12}$C and direct $\alpha$ transfer $^{12}$C ($^{16}$O,$^{12}$C)$^{16}$O channels shown in Fig. 1 are taken into account explicitly. The strength of the $\alpha$ transfer in the elastic $^{16}$O+$^{12}$C scattering is directly proportional to the probability of the dissociation of $^{16}$O into the $\alpha$ particle and $^{12}$C nucleus, i.e., the $\alpha$ spectroscopic factor $S_\alpha$ [26–29]. The $S_\alpha$ values deduced from the earlier CRC [21] and DWBA [22, 23] calculations, taking into account only the direct $\alpha$ transfer in the elastic $^{16}$O+$^{12}$C scattering, are much larger than those predicted by the SM and cluster model calculations [29, 30]. Such a disagreement clearly indicates that the higher-order, indirect $\alpha$ transfer contributions might not be negligible. For example, the indirect $\alpha$ transfer via the $2^+_1$ excitation of the $^{12}$C core is expected to be significant because of the large $S_\alpha$ values predicted by the SM and $\alpha$-cluster model calculations [26, 29–31] for the dissociation $^{16}$O$_{\text{g.s.}} \rightarrow \alpha + ^{12}$C$_{2^+_1}$. To shed more light on this problem, we have performed in the present work a multistep CRC analysis of the elastic $^{16}$O+$^{12}$C scattering, taking into account explicitly the contributions from both the direct and indirect $\alpha$ transfers (via the excited states of $^{12}$C and $^{16}$O), with the real OP and inelastic scattering form factors for the considered excited states given by the DFM [4, 32]. The $S_\alpha$ values predicted recently by the large scale SM calculation [29, 31] are used consistently in the present work. The possible CRC contributions of the nucleon transfer and indirect transfer of $^3$He and $^3$H clusters to the enhancement of the elastic $^{16}$O+$^{12}$C cross section at backward angles are also studied.

## II.   OPTICAL MODEL ANALYSIS OF THE ELASTIC $^{16}$O+$^{12}$C SCATTERING

Given the difficulty mentioned above in the OM description of the elastic $^{16}$O+$^{12}$C scattering at low energies, a proper choice of the complex, energy dependent OP for this system is a prerequisite for any CC or CRC study of the nonelastic processes induced by the $^{16}$O+$^{12}$C collision. While the elastic $^{16}$O+$^{12}$C data at backward angles might include the contribution from the $\alpha$ transfer, the Fraunhofer-type oscillation observed at forward angles is generated entirely by the elastic scattering, and a properly chosen OP for the $^{16}$O+$^{12}$C system should reproduce the forward-angle elastic data as accurately as possible. With the increasing energy, when more reaction channels are open, the enhancement of the elastic $^{16}$O+$^{12}$C cross section at large angles is gradually disappeared, giving rise to the exponential fall-off of the elastic cross section caused by a stronger absorption [19]. When the energy reaches the range of refractive energies of about 10 to 40 MeV/nucleon, the elastic $^{16}$O+$^{12}$C scattering

5

becomes strongly refractive and the nuclear rainbow appears. Such data are indispensable in validating the prediction of different theoretical methods, like the DFM which derives the real nucleus-nucleus OP from the realistic densities of the two colliding nuclei and appropriate nucleon-nucleon (NN) interaction between the projectile- and target nucleons. The recent (mean-field based) version of the DFM was shown [4] to account very well for the energy dependence of the real OP, and the (energy dependent) folded potential $U_F$ [4] obtained with the CDM3Y3 density dependent NN interaction [14] is used in the present OM analysis of the elastic $^{16}O+^{12}C$ scattering as the real OP. The imaginary (absorptive) OP is due to the open nonelastic channels, and is usually assumed in the standard WS form. Thus, the total OP at the internuclear distance $R$ is determined as

$$U(R) = N_R U_F(E, R) - \frac{iW_V}{1 + \exp[(R - R_V)/a_V]} + V_C(R). \tag{1}$$

The Coulomb potential $V_C(R)$ is obtained by folding two uniform charge distributions [33], chosen to have RMS charge radii $R_C = 3.17$ and $3.54$ fm for $^{12}C$ and $^{16}O$, respectively. Such a choice of the Coulomb potential was shown to be accurate up to small radii where the nuclear interaction becomes dominant [2]. The ground state (g.s.) densities of $^{16}O$ and $^{12}C$ used in the DFM calculation were taken as Fermi distributions with parameters [34] chosen to reproduce the empirical matter radii of these nuclei. The OM calculations were made using the code ECIS97 written by Raynal [35]. The renormalization factor $N_R$ of the real folded OP and parameters of the WS imaginary OP were adjusted by the best OM description of the elastic data, especially, the data points at the most forward angles.

Very helpful for the illustration of the refractive structure of the nuclear rainbow is the near-far decomposition of the elastic scattering amplitude based on the method developed by Fuller [36]. Namely, by decomposing the Legendre function $P_l(\cos\theta)$ into waves traveling in $\theta$ that are running in the opposite directions around the scattering center, the elastic amplitude $f(\theta)$ can be expressed in terms of the near-side ($f_N$) and far-side ($f_F$) components as

$$f(\theta) = f_N(\theta) + f_F(\theta) = \frac{i}{2k} \sum_l (2l+1) A_l \left[ \tilde{Q}_l^{(-)}(\cos\theta) + \tilde{Q}_l^{(+)}(\cos\theta) \right], \tag{2}$$

$$\text{where} \quad \tilde{Q}_l^{(\mp)}(\cos\theta) = \frac{1}{2} \left[ P_l(\cos\theta) \pm \frac{2i}{\pi} Q_l(\cos\theta) \right],$$

and $Q_l(\cos\theta)$ is the Legendre function of the second kind. The amplitude $f_N(\theta)$ represents the waves deflected to the direction of $\theta$ on the near side of the scattering center, and the
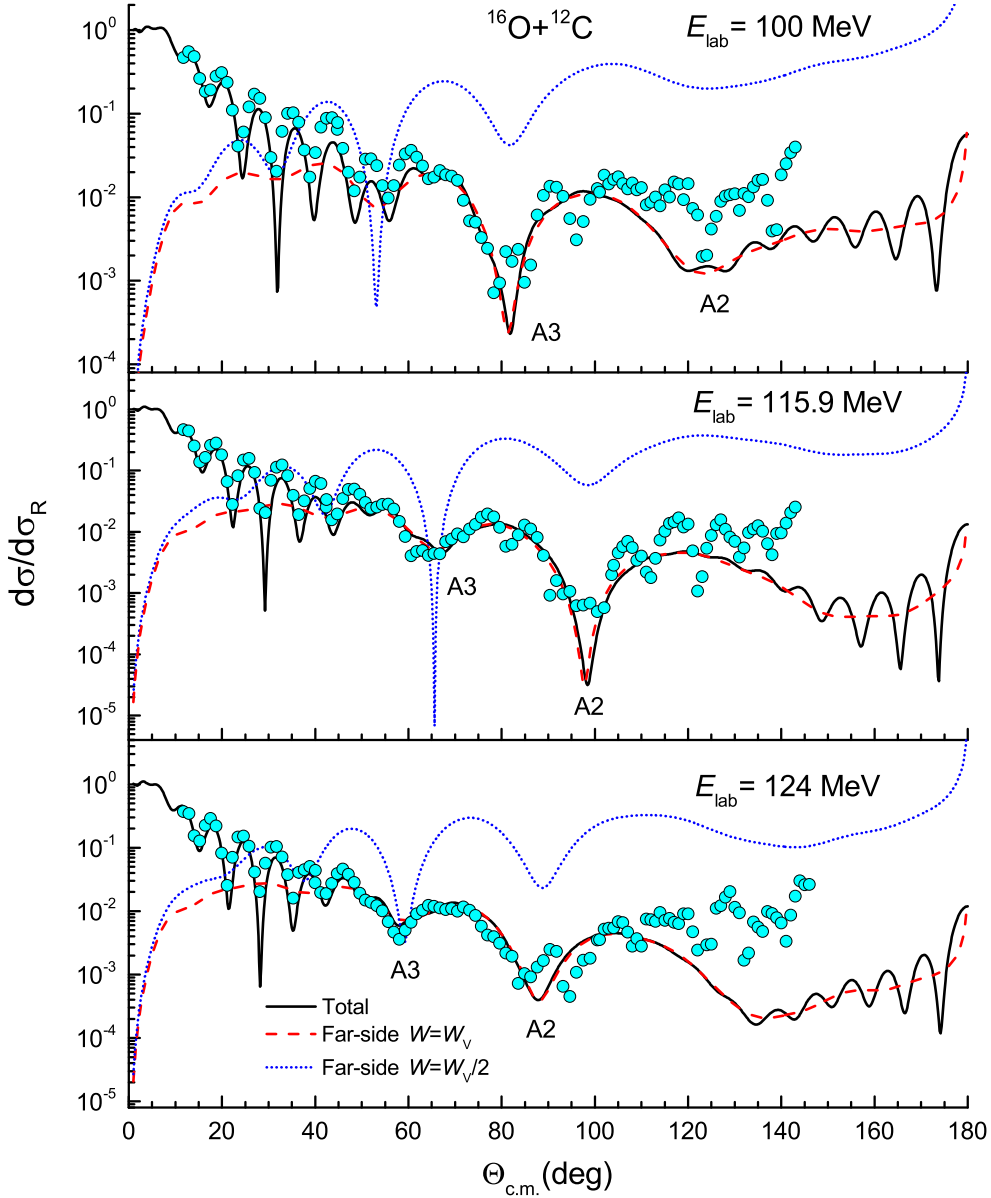
FIG. 2. OM description of the elastic $^{16}$O+$^{12}$C data at $E_{lab} = 100$, 115.9, and 124 MeV [11] given by the best-fit real folded OP and WS imaginary OP (see parameters in Table I). The far-side scattering cross sections are given by the near-far decomposition (2) using the same real folded OP but with different strengths $W_V$ of the WS imaginary OP (dashed and dotted lines). Ak is the k-th order Airy minimum.

waves traveling on the opposite, far side of the scattering center to the same angle $\theta$ give rise to the far-side amplitude $f_F(\theta)$. Therefore, the near-side scattering occurs mainly at the surface, while the far-side (refractive) scattering penetrates more into the interior of the nucleus-nucleus system. The broad oscillation of the far-side cross section is directly

TABLE I. The best-fit OP parameters (1) used in the OM analysis of the elastic $^{16}$O+$^{12}$C scattering at $E_{\text{lab}} = 100 - 300$ MeV. $J_R$ and $J_W$ are the volume integrals (per interacting nucleon pair) of the real and imaginary parts of the OP, respectively.

| $E_{\text{lab}}$ (MeV) | $N_R$ | $J_R$ (MeV fm$^3$) | $W_V$ (MeV) | $R_V$ (fm) | $a_V$ (fm) | $J_W$ (MeV fm$^3$) | $\sigma_R$ (mb) | Data |
|---|---|---|---|---|---|---|---|---|
| 100 | 1.006 | 332.1 | 11.21 | 6.020 | 0.52 | 57.0 | 1401 | [11] |
| 115.9 | 1.002 | 328.8 | 13.70 | 5.781 | 0.60 | 63.9 | 1464 | [11] |
| 124 | 1.000 | 327.1 | 14.50 | 5.800 | 0.60 | 68.2 | 1485 | [11] |
| 132 | 1.020 | 332.6 | 14.00 | 5.853 | 0.72 | 70.4 | 1638 | [9, 10] |
| 300 | 0.960 | 293.6 | 26.37 | 5.632 | 0.68 | 117.5 | 1655 | [12] |

associated with the Airy structure of the nuclear rainbow [3, 37].

The OM description of the elastic $^{16}$O+$^{12}$C scattering data at $E_{\text{lab}} = 100 - 124$ MeV is shown in Fig. 2. The realistic OP family obtained in the folding model analysis [4] of the elastic $^{16}$O+$^{12}$C scattering at the refractive energies was extrapolated to lower energies, and the best OM fit to the elastic data from the forward angles up to the center-of-mass (c.m.) angles around 100° has been achieved with the real folded OP renormalized by the factor $N_R$ close to unity (see Table I). The obtained volume integrals (per interacting nucleon pair) of the real ($J_R$) and imaginary ($J_W$) potentials agree well with the global systematics of the elastic scattering of light HI given by both the OM analysis of the elastic data and prediction by the dispersion relation that links the real and imaginary parts of the OP (see, e.g., Fig. 6.7 in Ref. [2]). Because the refractive Airy structure determined by the far-side scattering is frequently weakened by the absorption, the OM calculation was done also with a strength of the imaginary WS potential reduced by 50%, and the results (see the far-side cross sections shown in Fig. 2) reproduce nicely the broad Airy oscillation pattern established earlier in the OM analyses of the elastic $^{16}$O+$^{12}$C data over a wide range of energies [4, 10]. At low energies ($E_{\text{lab}} \lesssim 132$ MeV), the first Airy minimum A1 is located in the backward region and strongly distorted by a quickly oscillating cross section that is likely due to the elastic $\alpha$ transfer process [19, 20].

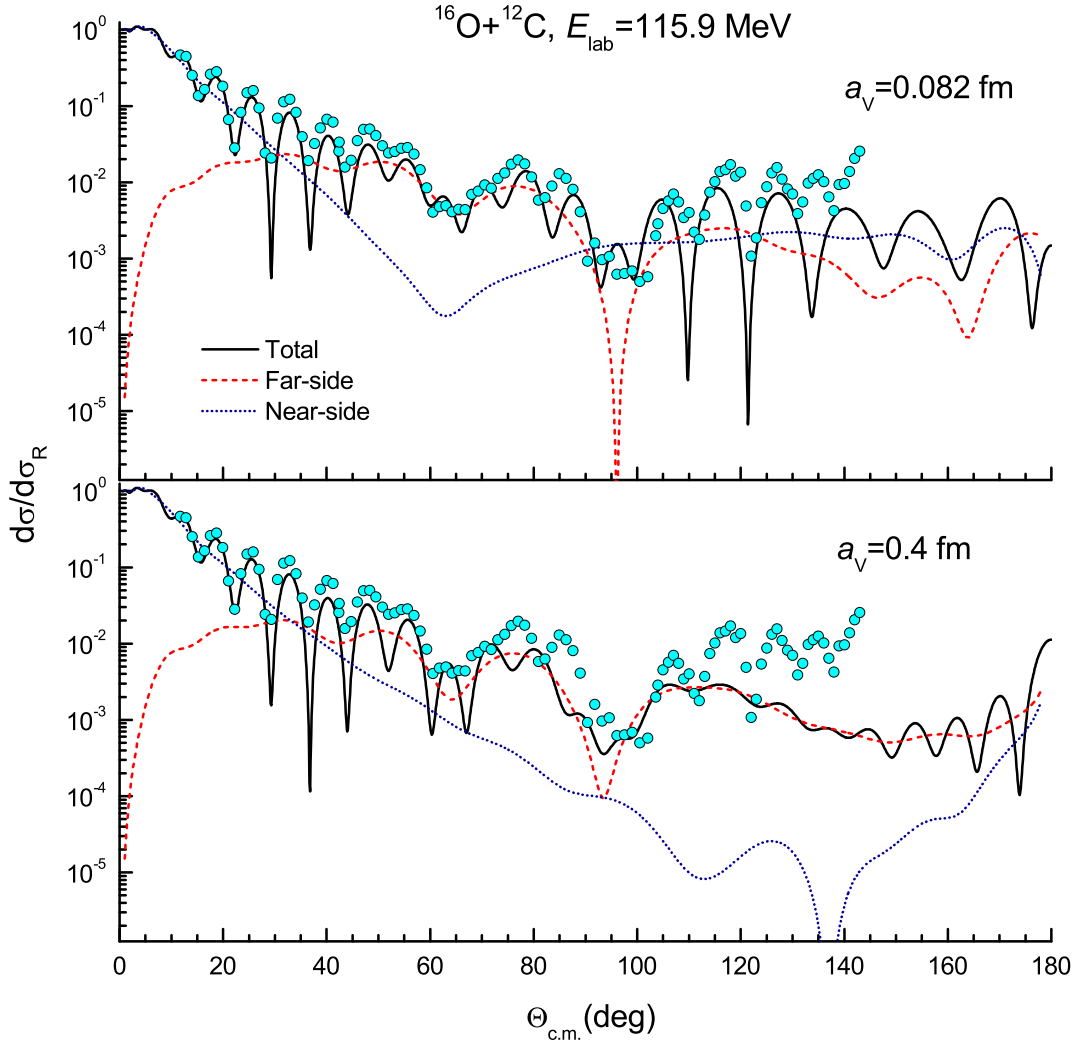In the OM description of the elastic $^{16}$O+$^{12}$C scattering, the quick Fraunhofer oscillation

FIG. 3. OM description of the elastic $^{16}$O+$^{12}$C data at $E_{lab} = 115.9$ MeV [11] given by the best-fit real folded OP and WS imaginary OP containing both the volume and surface terms (solid lines). The different behaviors of the near-side cross section at large angles are caused by two different values of the diffuseness $a_V$ of the volume WS term of the imaginary OP.

of the elastic cross section at the forward angles is well known to be due to the interference between the near-side and far-side scattering (2). Because the near-side scattering contributes mainly to the diffraction at forward angles, the near-far interference is usually weak at medium and large angles where only the far-side scattering amplitude survives [3]. However, the quickly oscillating cross section at large angles observed in the elastic $^{16}$O+$^{12}$C scattering at low energies (see Fig. 2) seems to result from some interference pattern that

distorts the smooth far-side cross section there. The original OM analysis of these data by Nicoli *et al.* [11] based on different choices of the OP, including the model-independent spline shape for the real OP, has shown that the observed oscillatory enhancement of the elastic cross section at backward angles can be reproduced only with a very *small diffuseness* of the WS imaginary OP.

To illustrate this effect, we have performed the OM calculation using the same best-fit real folded OP and WS imaginary OP containing both the volume and surface terms as that used in Ref. [11], with parameters adjusted by the best OM fit to the data. The best-fit WS parameters turned out to be quite close to those obtained in Ref. [11], with a very small diffuseness $a_V \approx 0.08$ fm of the volume WS term. From the OM results shown in the upper panel of Fig. 3 one can see that the main impact by such a small diffuseness of the WS term is the unusually enhanced strength of the near-side scattering at backward angles, and the near-far interference gives rise then to the enhanced oscillation of the elastic cross section. Keeping the same WS imaginary OP but with a larger $a_V \approx 0.4$ fm, the near-side scattering is weakened substantially and the OM calculation fails again to describe the oscillating cross section at large angles (see lower panel of Fig. 3). In general, the near-side (surface) scattering occurs mainly at forward angles, and to boost the strength of the near-side scattering at backward angles using the WS absorptive potential with an extremely small diffuseness is just a computational technique to reproduce the enhanced oscillation of the elastic $^{16}$O+$^{12}$C cross section at backward angles, without any physics explanation of that phenomenon.

While a widely expected physics scenario in this case is the strong contribution from the $\alpha$ transfer channels to the elastic $^{16}$O+$^{12}$C scattering [19, 20], Ohkubo and Hirabayashi [25] have proposed a different scenario in their recent CC study of the elastic $^{16}$O+$^{12}$C scattering at $E_{\mathrm{lab}} = 115.9$ MeV, where the oscillatory pattern at large angles was interpreted as a result of the interference between the elastic scattering wave and "external reflective" wave (caused by the nuclear excitations taken into account in the CC calculation). A closer look at these results finds that such an external reflective wave is caused also by a small diffuseness ($a_V \approx 0.2$ fm) of the volume WS imaginary potential used in the CC calculation, because the same CC calculation using a larger diffuseness $a_V \approx 0.4$ fm (see Fig. 3 in Ref. [25]) fails again to describe the large-angle oscillation of the elastic cross section, in a manner similar to that shown in the lower panel of Fig 3.

## III. CRC STUDY OF THE ELASTIC ALPHA TRANSFER $^{12}$C ($^{16}$O,$^{12}$C)$^{16}$O

It is well established that the elastic scattering of nearly identical nuclei at low energies often involves the elastic transfer [38], which gives rise to a quickly oscillating elastic cross section at backward angles. For the $^{16}$O+$^{12}$C system, the elastic $\alpha$ transfer from $^{16}$O to $^{12}$C leads to the final state that is indistinguishable from that of the true elastic $^{16}$O+$^{12}$C scattering (see Fig. 1). Therefore, the total elastic amplitude should be a coherent sum of the elastic scattering amplitude $f_{\mathrm{ES}}$ and elastic $\alpha$ transfer amplitude $f_{\mathrm{ET}}$. The interference between $f_{\mathrm{ES}}$ and $f_{\mathrm{ET}}$ gives rise to the oscillatory elastic cross section at large angles, which is essentially the oscillation due to the symmetry of the two identical $^{12}$C cores [20, 38]. Given the significant $\alpha$ spectroscopic factors predicted by the large scale SM calculation [29] for different paths of the dissociation of $^{16}$O into $\alpha$-particle and the $^{12}$C core, the coupled channel contribution from the direct and indirect $\alpha$ transfers to the total elastic $^{16}$O+$^{12}$C cross section should be significant at low energies. Therefore, we have performed in the present work a detailed CRC analysis of the elastic $^{16}$O+$^{12}$C scattering at the energies $E_{\mathrm{lab}} = 100 - 300$ MeV, taking into account explicitly the couplings between the elastic scattering channel and different $\alpha$ transfer channels using the code FRESCO written by Thompson [39].

### A. CRC formalism

We give here a brief description of the multichannel CRC method to study the contributions of different $\alpha$ transfer channels to the elastic $^{16}$O+$^{12}$C scattering. In general, the coupled equation in the post form for a particular channel $\beta$ can be written as

$$(E_\beta - T_\beta - U_\beta)\chi_\beta = \sum_{\beta' \neq \beta, x = x'} \langle \beta | V | \beta' \rangle \chi_{\beta'} + \sum_{\beta' \neq \beta, x \neq x'} [\langle \beta | W_{\beta'} | \beta' \rangle + \langle \beta | \beta' \rangle (T_{\beta'} + U_{\beta'} - E_{\beta'})] \chi_{\beta'}, \quad (3)$$

where $\beta'$ is the scattering or transfer channel different from $\beta$, $x$ and $x'$ are the partitions associated with the considered transfer process. $\chi_\beta$ and $\chi_{\beta'}$ are the relative-motion wave functions while $U_\beta$ and $U_{\beta'}$ are the (diagonal) optical potentials in these two channels. Due to the identity of the entrance and exit channels, all post form formulas are equivalent to the prior ones, and the transfer interactions $W_\beta$ can be determined [27, 28] as

$$W_\beta = V_{\alpha + ^{12}\mathrm{C}} + (U_{^{12}\mathrm{C} + ^{12}\mathrm{C}} - U_{^{16}\mathrm{O} + ^{12}\mathrm{C}}), \quad (4)$$

where ($U_{^{12}C+^{12}C} - U_{^{16}O+^{12}C}$) is the complex remnant term which is the difference between the core-core OP and that of the exit channel. $V_{\alpha+^{12}C}$ is the binding potential of the $\alpha$ cluster inside the $^{16}O$ nucleus, which has been assumed in the standard WS form in our CRC calculation. The CRC equations (3)-(4) are solved iteratively, with the finite-range complex remnant terms and non-orthogonality corrections properly taken into account [39]. The diagonal OP for the considered channels are determined by Eq. (1) using the real double-folded potential [4] and WS imaginary potential. The (complex) inelastic scattering form factors for the nuclear transitions considered in the CRC study are also obtained in the DFM calculation [32] using the same CDM3Y3 interaction [4], with a complex density dependence suggested in Ref. [40]. For the $\alpha$ transfer, the internal state of the bound $\alpha$ cluster is assumed to be $1s$ state. Then, the relative-motion wave function $\Phi_{NL}(\boldsymbol{r}_{\alpha+^{12}C})$ of the $\alpha+^{12}C$ system ($L$-wave state) has the number of radial nodes $N$ determined by the Wildermuth condition [27, 28], so that the total number of the oscillator quanta $\mathcal{N}$ is conserved

$$\mathcal{N} = 2(N-1) + L = \sum_{i=1}^{4} 2(n_i - 1) + l_i, \tag{5}$$

where $n_i$ and $l_i$ are the principal quantum number and orbital momentum of each constituent nucleon in the $\alpha$ cluster. Using the fixed WS geometry ($R = 4.148$ fm and $a = 0.55$ fm in the 2-channel CRC calculation of the direct $\alpha$ transfer; $R = 3.683$ fm and $a = 0.55$ fm in the multi-channel CRC calculation of the direct and indirect $\alpha$ transfer) the wave function $\Phi_{NL}(\boldsymbol{r}_{\alpha+^{12}C})$ is obtained with the depth of the WS potential adjusted to reproduce the $\alpha$ separation energy $E_\alpha$ given by the relation

$$E_\alpha(J_i^\pi) = E_\alpha(\text{g.s.}) - E(^{16}O^*) + E(^{12}C^*), \tag{6}$$

where the $\alpha$ separation energy of $^{16}O$ in the ground state is $E_\alpha(\text{g.s.}) = 7.162$ MeV [41], $E(^{16}O^*)$ and $E(^{12}C^*)$ are the excitation energies of $^{16}O$ and the $^{12}C$ core, respectively. The solutions $\chi_\beta$ of the CRC equations (3)-(5) are used to determine the elastic scattering $f_{ES}$ and $\alpha$ transfer $f_{ET}$ amplitudes. The total elastic $^{16}O+^{12}C$ cross section is given [39] by

$$\frac{d\sigma(\theta)}{d\Omega} = |f(\theta)|^2 = |f_{ES}(\theta) + f_{ET}(\pi - \theta)|^2, \tag{7}$$

where the elastic $\alpha$ transfer amplitude at the c.m. angle ($\pi - \theta$) is coherently added to the elastic scattering amplitude at the c.m. angle $\theta$ (as illustrated in Fig. 1).

12

The CRC calculation requires the input of the spectroscopic amplitude $A_{NL}$ [26] which is used to construct the dinuclear overlap as

$$\langle {}^{12}\text{C}|{}^{16}\text{O}\rangle = A_{NL}({}^{16}\text{O}, {}^{12}\text{C})\Phi_{NL}(\boldsymbol{r}_{\alpha+{}^{12}\text{C}}). \tag{8}$$

The $\alpha$ spectroscopic factor is then determined as $S_\alpha = |A_{NL}|^2$. In the present CRC analysis, we have used $S_\alpha$ predicted recently by the large scale SM calculation, the so-called cluster-nucleon configuration interaction model [29, 31]. In this approach, $S_\alpha$ of ${}^{16}\text{O}$ has been obtained in the unrestricted single-nucleon $p$-$sd$ configuration space, using the realistic SM Hamiltonian and new definition of $S_\alpha$. The norm kernel originating from the full anti-symmetrization and orthonormalization of the multinucleon clustering wave functions was found to be very substantial, which increases $S_\alpha$ for ${}^{16}\text{O}$ in the g.s. from around 0.29 as given by the traditional definition of $S_\alpha$ (see Table I of Ref. [42] and discussion thereafter) to 0.794 (see Table III of Ref. [29]). In fact, the use of $S_\alpha$ determined in the traditional SM method was questioned some 40 years ago by Fliessbach [43, 44], and a new definition of the cluster spectroscopic factor similar to that adopted in Ref. [29] was used in the microscopic cluster decay study [45, 46]. Although it was shown years ago [47] that the use of the new definition of $S_\alpha$ in a transfer reaction calculation does not require any reformulation of the DWBA or CRC formalism, the present CRC calculation seems to be the first attempt to use the newly defined $S_\alpha$ in the study of the $\alpha$ transfer reaction.

### B. Direct $\alpha$ transfer

The observed oscillatory enhancement of the elastic ${}^{16}\text{O}+{}^{12}\text{C}$ cross section at large angles was repeatedly discussed in the past as due to the contribution from the elastic $\alpha$ transfer [19, 20, 38]. A straightforward method to estimate the strength of the direct (elastic) $\alpha$ transfer in the elastic ${}^{16}\text{O}+{}^{12}\text{C}$ scattering is to add the elastic $\alpha$ transfer amplitude in the DWBA to the elastic scattering amplitude [22, 23]. A more consistent approach is to solve the CRC equations (3)-(6), coupling explicitly the elastic scattering and direct $\alpha$ transfer channels [21]. We discuss briefly here the results of our CRC calculation of the direct $\alpha$ transfer using the (real folded + imaginary WS) optical potentials (1) for the ${}^{16}\text{O}+{}^{12}\text{C}$ and ${}^{12}\text{C}+{}^{12}\text{C}$ systems. Assuming the $\alpha$-clustering of the $p$-shell nucleons in ${}^{16}\text{O}$, the direct elastic $\alpha$ transfer proceeds via the $S$ state ($L = 0$) of the $\alpha+{}^{12}\text{C}$ system, which implies $N = 3$ in
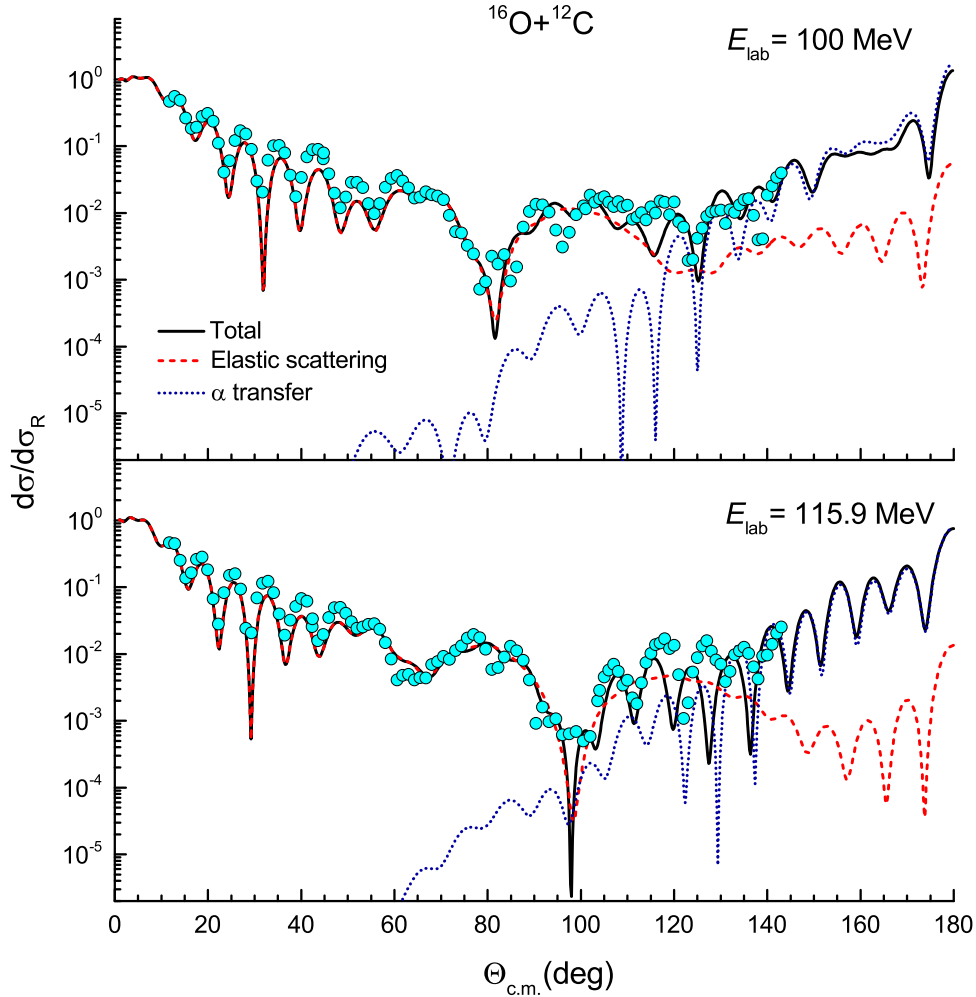
13

FIG. 4. CRC description (solid lines) of the elastic $^{16}$O+$^{12}$C data measured at $E_{\text{lab}} = 100$ and 115.9 MeV [11]. The true elastic scattering cross section (dashed lines) are obtained with the real folded potential and WS imaginary potential taken from Table I. The elastic $\alpha$ transfer cross section (dotted lines) are given by the best-fit $\alpha$ spectroscopic factor $S_\alpha \approx 1.96$.

the Wildermuth's rule (5) including the origin and excluding the infinity. In this case, the WS depth of the $\alpha$ binding potential was adjusted to reproduce the $\alpha$ separation energy $E_\alpha(\text{g.s.}) \approx 7.162$ MeV. The total elastic $^{16}$O+$^{12}$C cross sections given by the present CRC calculation are compared with the elastic $^{16}$O+$^{12}$C data measured at $E_{\text{lab}} = 100 - 300$ MeV [9–12] in Figs. 4 and 5. The use of the $\alpha$ spectroscopic factor predicted by the SM [29] gives a very weak elastic transfer cross section that cannot account for the enhanced oscillating cross section at backward angles. It is an indication of the strong contribution from the indirect $\alpha$ transfer to the elastic $^{16}$O+$^{12}$C cross section. A simple (effective) way of the

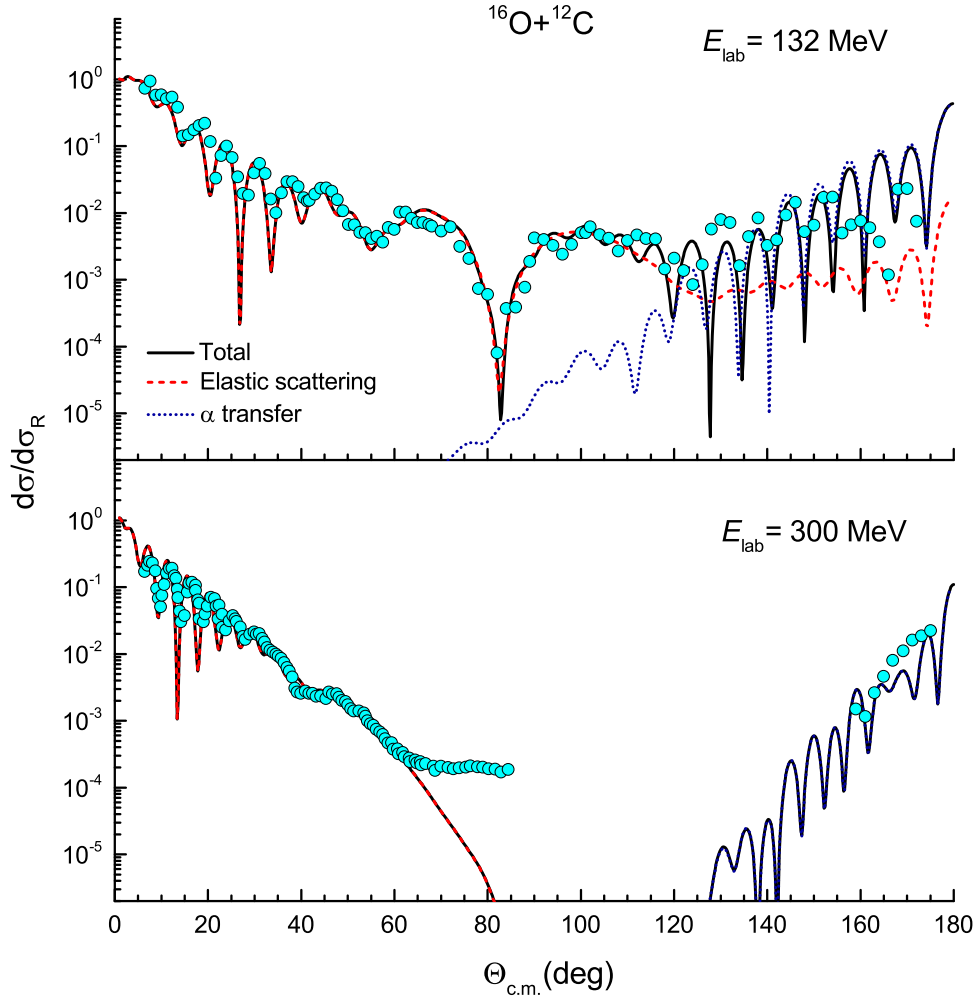FIG. 5. The same as Fig. 4 but for the elastic $^{16}$O+$^{12}$C data measured at $E_{\text{lab}} = 132$ [9, 10], and 300 MeV [12].

.

DWBA or CRC analysis of the direct transfer reaction is to treat the cluster spectroscopic factor as a free parameter to be adjusted to the best fit of the transfer data. In such an approach, our CRC calculation gives consistently a good description of the elastic $^{16}$O+$^{12}$C data at different energies using the same $\alpha$ spectroscopic factor $S_\alpha \approx 1.96$ for the g.s. of $^{16}$O (see Figs. 4 and 5). The explicit comparison of the true elastic $^{16}$O+$^{12}$C scattering and direct $\alpha$ transfer shows that the oscillatory enhancement of the elastic cross section at backward angles is due to the elastic $\alpha$ transfer $^{12}$C $(^{16}$O,$^{12}$C$)^{16}$O process. We also found that the back coupling from the direct $\alpha$ transfer to the elastic $^{16}$O+$^{12}$C scattering at forward angles is not significant, and the same complex OP's as those used in the OM calculation discussed

in Section II (see Table I) can be used in the CRC calculation. We note that the data points at the most backward angles measured at $E_{lab} = 300$ MeV [12] are described by the present CRC result as due entirely to the elastic $\alpha$ transfer. We have considered these data points in the OM analysis of the elastic $^{16}O+^{12}C$ scattering at 300 MeV, and they cannot be described by the standard OM calculation, despite a broad variation of the strength and shape of the complex OP. Consequently, the 300 MeV data points at the most backward angles can be used to gauge the strength of the $\alpha$ spectroscopic factor in the CRC analysis of the elastic $^{16}O+^{12}C$ scattering. The best-fit $S_\alpha \approx 1.96$ obtained in the 2-channel CRC analysis agrees reasonably with that deduced earlier (see Table II) from the DWBA and CRC studies of the elastic $^{16}O+^{12}C$ scattering at low energies. However, most of the empirical values of the

TABLE II. $\alpha$ spectroscopic factor $S_\alpha$ deduced from the 2-channel CRC analysis of the elastic scattering and direct $\alpha$ transfer in the $^{16}O+^{12}C$ system, in comparison with that deduced earlier from the DWBA and CRC studies of the elastic $\alpha$ transfer reaction $^{12}C$ $(^{16}O,^{12}C)^{16}O$.

| $E_{lab}$ (MeV) | $S_\alpha$ | Reference |
|---|---|---|
| $100 - 300$ | 1.96 | Present work |
| $20 - 35$ | $1.0 - 1.96$ | [20] |
| $100 - 124$ | $1.21 - 1.96$ | [21] |
| $20 - 132$ | $1.45 - 1.58$ | [22] |
| $132, 181$ | $0.49 - 0.81$ | [48] |
| $28 - 61.5$ | $1.59 - 3.00$ | [49] |

$\alpha$ spectroscopic factor $S_\alpha$ shown in Table II seem to be much larger than that predicted by the recent large scale SM calculation ($S_\alpha \approx 0.8$) [29] or $4\alpha$ cluster model ($S_\alpha \approx 0.6$) [30].

## C. Indirect $\alpha$ transfer via the excited states of $^{16}O$ and the $^{12}C$ core

The scenario of the direct $\alpha$ transfer presented in Sec. III B is sound but the question remains about the obtained $\alpha$ spectroscopic factor $S_\alpha \approx 1.96$ that is more than twice that predicted by the SM calculation [29] or $4\alpha$ cluster model of $^{16}O$ [30]. Obviously, the various indirect $\alpha$ transfer channels via the excited states of $^{16}O$ and the $^{12}C$ core should also contribute to the total elastic $\alpha$ transfer. For example, the elastic $\alpha$ transfer in the $^{16}O+^{12}C$

system was predicted by the cluster models [26, 30] to proceed also indirectly through the $2_1^+$ excited state of the $^{12}$C core. In general, it is necessary to consider the indirect $\alpha$ transfer in a sufficiently large model space consisting of the most important excited states of $^{16}$O [24]. The $0_2^+$ (6.05 MeV) and $2_1^+$ (6.92 MeV) states of $^{16}$O are the low-lying members of the $K^\pi = 0^+$ rotational band with a well-developed $\alpha+^{12}$C cluster structure [50], and they are expected to have a non-negligible contribution to the $\alpha$ transfer in the elastic $^{16}$O+$^{12}$C scattering. The $3_1^-$ (6.13 MeV) state has a SM-type structure similar to the g.s. of $^{16}$O, but it can have a strong coupling effect caused by a large octupole transition strength. The $0_2^+$, $3_1^-$, $2_1^+$ excited states of $^{16}$O were also predicted by the large scale SM [29] to have the $\alpha$ spectroscopic factor $S_\alpha \approx 0.535$, 0.663, and 0.5, respectively, which are comparable with $S_\alpha \approx 0.794$ predicted for the g.s. of $^{16}$O. The other excited states of $^{16}$O are at the higher energies, with the $\alpha$ spectroscopic factors (see Table III in Ref. [29]) predicted to be much smaller than those mentioned above. Therefore, we have tried in the present multichannel CRC analysis of the elastic $^{16}$O+$^{12}$C scattering to explore the impact of the indirect $\alpha$ transfer through the $0_2^+$, $3_1^-$, and $2_1^+$ excited states of $^{16}$O as well as the $2_1^+$ state of the $^{12}$C core. The explicit coupling scheme of the 10 reaction channels considered in the present work is shown in Fig. 6.

To study the indirect $\alpha$ transfers via the excited states of $^{16}$O in the CRC analysis with the coupling scheme shown in Fig. 6, the dinuclear overlap is determined by the same relation (8), where the orbital momentum $L$ of the relative-motion wave function $\Phi_{NL}(\boldsymbol{r}_{\alpha+^{12}\mathrm{C}})$ is assumed to be equal the spin of the excited state of $^{16}$O. For a consistent test of the $\alpha$ spectroscopic factors predicted recently in the large scale SM calculation by Volya and Tchuvilsky [29, 31] that treats the cluster channel wave function in a translationally invariant manner [42], we have used these $S_\alpha$ values as fixed parameters in our CRC analysis of the elastic $^{16}$O+$^{12}$C scattering. The summary of the CRC inputs for the g.s. and excited states of $^{16}$O is given in Table III. The complex inelastic $^{16}$O$_{\mathrm{g.s.}} \rightarrow ^{16}$O$^*$ form factors were calculated in the generalized DFM [32], using the transition densities of the $0_2^+$, $3_1^-$, and $2_1^+$ states obtained in the Orthogonality Condition Model (OCM) by Okabe [51] and the complex CDM3Y3 density dependent interaction [4]. The OCM transition densities were slightly renormalized to reproduce the measured transition strengths [52], M(E0) $= 3.55 \pm 0.21$ $e$ fm$^2$, B(E3) $= 1490 \pm 70$ $e^2$fm$^6$, and B(E2) $= 39.3 \pm 1.6$ $e^2$fm$^4$ of the $0_2^+$, $3_1^-$, and $2_1^+$ states, respectively.

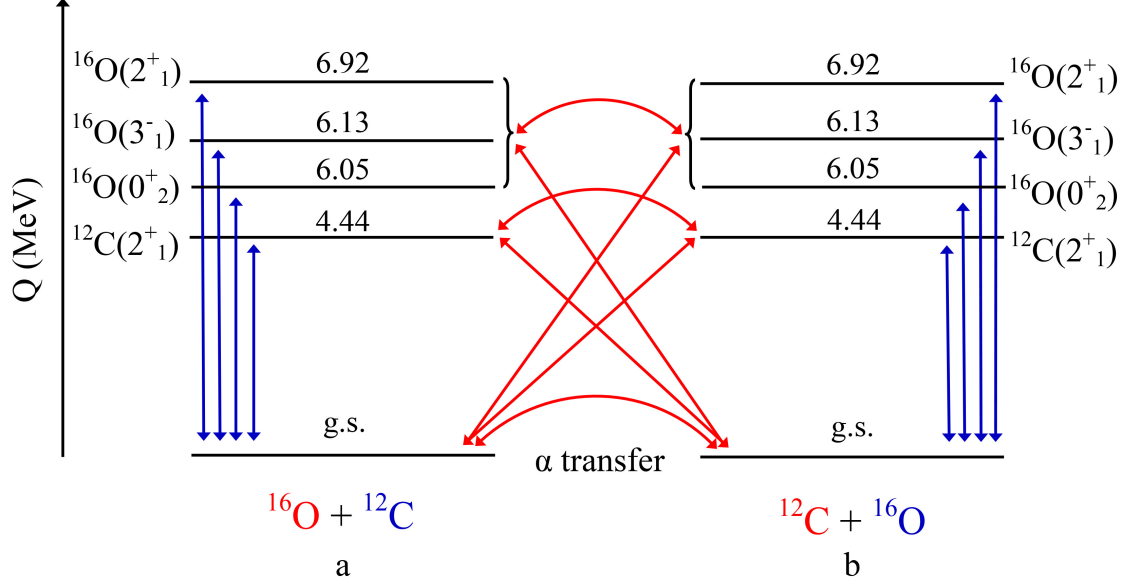The dissociation of $^{16}$O into the $\alpha+^{12}$C$_{2_1^+}$ configuration has been discussed earlier in the

17

FIG. 6. Coupling scheme of the 10 reaction channels taken into account in the present CRC analysis of the elastic $^{16}$O+$^{12}$C scattering that includes both the direct and indirect $\alpha$ transfer processes (see details in text).

TABLE III. $S_\alpha$ values used in our CRC analysis of the direct and indirect $\alpha$ transfer via the g.s. and excited states of $^{16}$O were taken from the results of the large scale SM calculation [29]. The number of radial nodes $N$ and orbital momentum $L$ of the corresponding $\alpha+^{12}$C configurations are given by the Wildermuth rule (5).

| $J^\pi$ | $E_x$ (MeV) | $N$ | $L$ | $S_\alpha$ |
|---|---|---|---|---|
| $0_1^+$ | 0.000 | 3 | 0 | 0.794 |
| $0_2^+$ | 6.049 | 5 | 0 | 0.535 |
| $3_1^-$ | 6.130 | 2 | 3 | 0.663 |
| $2_1^+$ | 6.917 | 4 | 2 | 0.500 |

SM and nuclear cluster studies [26, 30, 53–55]. Given $^{16}$O in its g.s., we need to input $N = 2$ and $L = 2$ into the Wildermuth's rule (5) for the $\alpha+^{12}$C$_{2_1^+}$ configuration. According to the SM studies [26, 29, 31, 54, 55] the $2_1^+$ and g.s. of $^{12}$C are of the same SU(3) shell structure ($\alpha$ composed of the same clustering nucleons coupled to the $^{12}$C core in its g.s. or an excited

18

states) and should have, therefore, the same $\alpha$ spectroscopic factor. However, this $S_\alpha$ value must be enhanced by the number of the possible $M$-substates of the $\alpha+^{12}C_{2_1^+}$ configuration [26], so that

$$A_{NL}^2(^{16}O_{\text{g.s.}}, ^{12}C^*(L)) = (2L+1)A_{N=3,L=0}^2(^{16}O_{\text{g.s.}}, ^{12}C_{\text{g.s.}}). \tag{9}$$

As a result, we obtain the enhancement factor of 5 for the $\alpha$ spectroscopic factor of the $2_1^+$ state of $^{12}C$ compared to that of $^{12}C_{\text{g.s.}}$ [26, 31, 55]. Given $S_\alpha \approx 0.794$ for the dissociation $^{16}O_{\text{g.s.}} \to \alpha+^{12}C_{\text{g.s.}}$ predicted by the large scale SM calculation [29, 31], one finds from the relation (9) that $S_\alpha \approx 3.9$ for the dissociation $^{16}O_{\text{g.s.}} \to \alpha+^{12}C_{2_1^+}$. This value was used as a fixed parameter in the present CRC calculation. Beside the SM results, the cluster $\alpha+^{12}C$ configurations of $^{16}O$ have been studied also in the OCM by Suzuki [53], and recently in the $4\alpha$ cluster OCM model by Yamada $et$ $al.$ [30]. The $S_\alpha$ values predicted by different structure models [29–31, 53] for the $\alpha+^{12}C_{2_1^+}$ configuration are of 3 to 5 times that predicted for the $\alpha+^{12}C_{\text{g.s.}}$ configuration (see Table IV), and this is clearly due to the degeneracy of the $M$-substates. For $^{12}C$ in the $3_1^-$ state at 9.6 MeV, the total number of the oscillator quanta $\mathcal{N}$ for the configuration $\alpha+^{12}C_{3_1^-}$ is not conserved, because $N$ is implied by the Wildermuth's rule (5) to be half-integer. Therefore, it cannot contribute to the $\alpha$ transfer cross section. Another important state of the $^{12}C$ core is the $0_2^+$ excitation at 7.65 MeV (Hoyle state), but $S_\alpha \approx 0.06$ predicted [55] for the dissociation $^{16}O_{\text{g.s.}} \to \alpha+^{12}C_{0_2^+}$ is too small to make any contribution to the indirect $\alpha$ transfer. This result also agrees with the $\alpha$ pickup data [56–58] where $S_\alpha$ obtained for the $\alpha+^{12}C_{0_2^+}$ configuration is nearly 4 times smaller than that of the $\alpha+^{12}C_{\text{g.s.}}$ configuration. In fact, the loosely bound $3\alpha$ structure of the Hoyle state leads to a fragile $\alpha+^{12}C_{0_2^+}$ configuration in $^{16}O$ that is strongly mixed with the $4_2^+$ state of $^{16}O$ at the energy above 18 MeV [50], which is mainly of $4\alpha$ structure and lying too high for the back coupling to the $\alpha$ transfer channel in the elastic $^{16}O+^{12}C$ scattering. Therefore, we did not include the $0_2^+$ state of the $^{12}C$ core in our CRC calculation. The complex inelastic $^{12}C_{\text{g.s.}} \to ^{12}C_{2_1^+}$ form factor was also calculated in the generalized DFM [32], using the $2_1^+$ transition density obtained in the Resonating Group Method (RGM) by Kamimura [59]. This choice of the $2_1^+$ transition density has been well tested in the earlier folding model analysis of the inelastic $\alpha+^{12}C$ scattering at different energies [40].

The total elastic $^{16}O+^{12}C$ cross sections given by the present CRC calculation are compared with the data measured at $E_{\text{lab}} = 100 - 300$ MeV [9–12] in Figs. 7 and 8. At variance with the CRC calculation of the direct $\alpha$ transfer discussed in Sect. III B, the 10-channel cou-

TABLE IV. $\alpha$ spectroscopic factors predicted by different structure models for the dissociation $^{16}\text{O} \to \alpha + ^{12}\text{C}$, where the $^{12}\text{C}$ core is in its ground state and $2_1^+$ excited state at 4.44 MeV. The $S_\alpha$ values used in the present CRC analysis of the elastic $^{16}\text{O}+^{12}\text{C}$ scattering (shown in the last row) were obtained in the large scale SM calculation [29, 31].

| | $S_\alpha$ | | |
|---|---|---|---|
| Model | $\alpha+^{12}\text{C}_{\text{g.s.}}$ | $\alpha+^{12}\text{C}_{2_1^+}$ | Reference |
| SM | 0.228 | 1.265 | [54] |
| SM | 0.235 | 1.30 | [55] |
| SM | 0.296 | 1.48 | [26] |
| OCM | 0.30 | 1.397 | [53] |
| $4\alpha$-OCM | 0.59 | 1.47 | [30] |
| SM | 0.794 | 3.90 | [29, 31] |

pling shown in Fig. 6 was found to affect the complex OP for the elastic $^{16}\text{O}+^{12}\text{C}$ scattering significantly, especially, the coupling to the $2_1^+$ excitation of the $^{12}\text{C}$ core as found earlier in the folding model analysis of the inelastic $\alpha+^{12}\text{C}$ scattering [40]. The OP parameters were readjusted mainly for the best CRC fit to the elastic $^{16}\text{O}+^{12}\text{C}$ data at forward angles which are of the true elastic scattering. One can see in Table V that the absorption strength of the imaginary WS potential was reduced substantially at the considered energies due to the explicit coupling to the nonelastic channels shown in Fig.6. To reveal the contributions of different elastic $\alpha$ transfer paths to the elastic $^{16}\text{O}+^{12}\text{C}$ cross section at large angles, we have performed several CRC calculations with different coupling schemes. The dash-dotted lines in Figs. 7 and 8 represent the results of the CC calculation of the elastic $^{16}\text{O}+^{12}\text{C}$ scattering with only the coupling to the excited states in the initial partition (a) included, neglecting the $\alpha$ transfer. The dotted lines show the results of the CRC calculation including the direct elastic $\alpha$ transfer between the initial partition (a) and its $\alpha$-exchanged counterpart (b). The dashed lines show the results of the CRC calculation including contributions from both the direct $\alpha$ transfer and indirect $\alpha$ transfer via the $2_1^+$ state of the $^{12}\text{C}$ core. Finally, the solid lines in Figs. 7 and 8 show the results of the full CRC calculation including different $\alpha$-transfer paths between the considered 10 channels. We note that the number of channels labeled in the figure legends corresponds to the number of reaction channels involving the $\alpha$
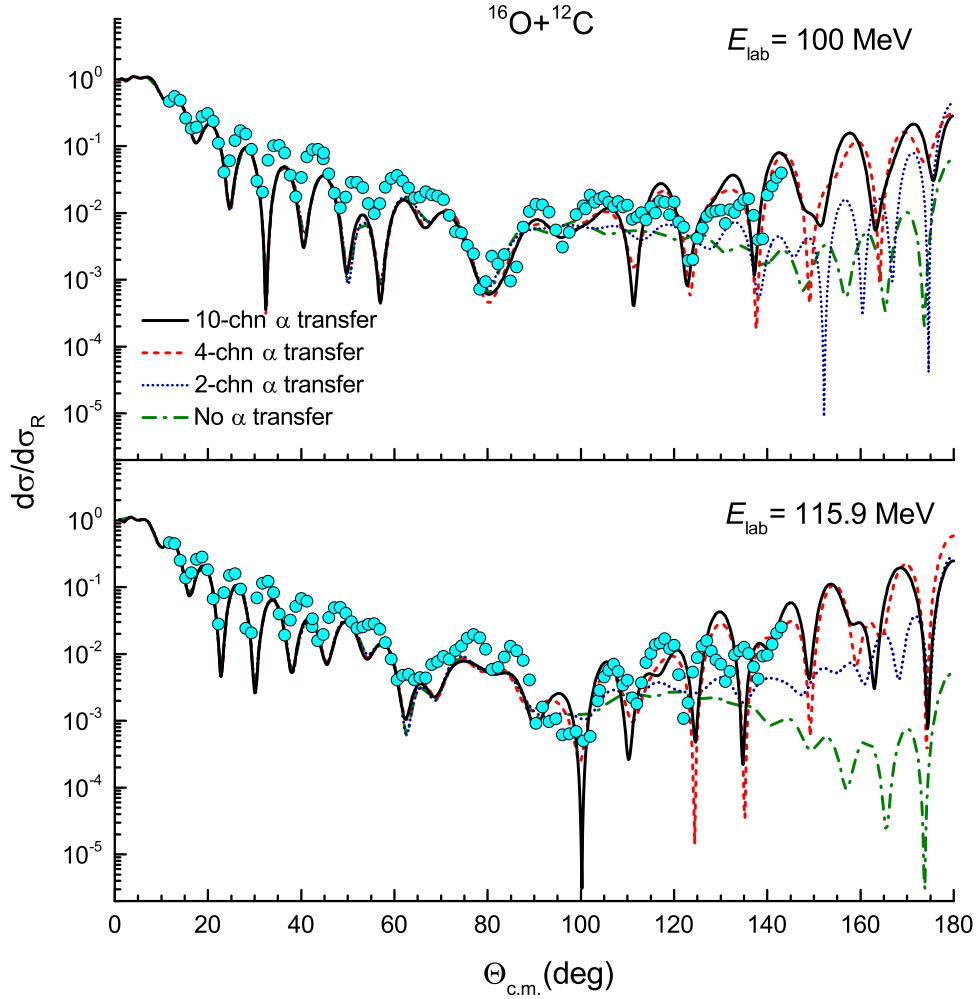
FIG. 7. Full CRC description of the elastic $^{16}$O+$^{12}$C scattering data measured at $E_{\mathrm{lab}} = 100$ and 115.9 MeV [11] (solid lines) in comparison with the CC results for purely elastic scattering, neglecting the $\alpha$ transfer (dash-dotted lines), the CRC results including the (direct) 2-channel $\alpha$ transfer (dotted lines), and the CRC results including the (direct and indirect via the $2^+_1$ state of the $^{12}$C core) 4-channel $\alpha$ transfer (dashed lines). See more details in text.

transfer between the two partitions (a) and (b). For each partition, the inelastic scattering channels were always coupled to the elastic scattering channel in all the CRC calculations discussed here.

One can see in Figs. 7 and 8 that without the contribution from the $\alpha$ transfer channels the CC calculation alone (dash-dotted lines) could describe the elastic $^{16}$O+$^{12}$C scattering at the forward- and medium angles only. A clear evidence of the failure of the CC method are the results shown in Fig. 8 for the elastic $^{16}$O+$^{12}$C scattering at $E_{\mathrm{lab}} = 300$ MeV where the elastic
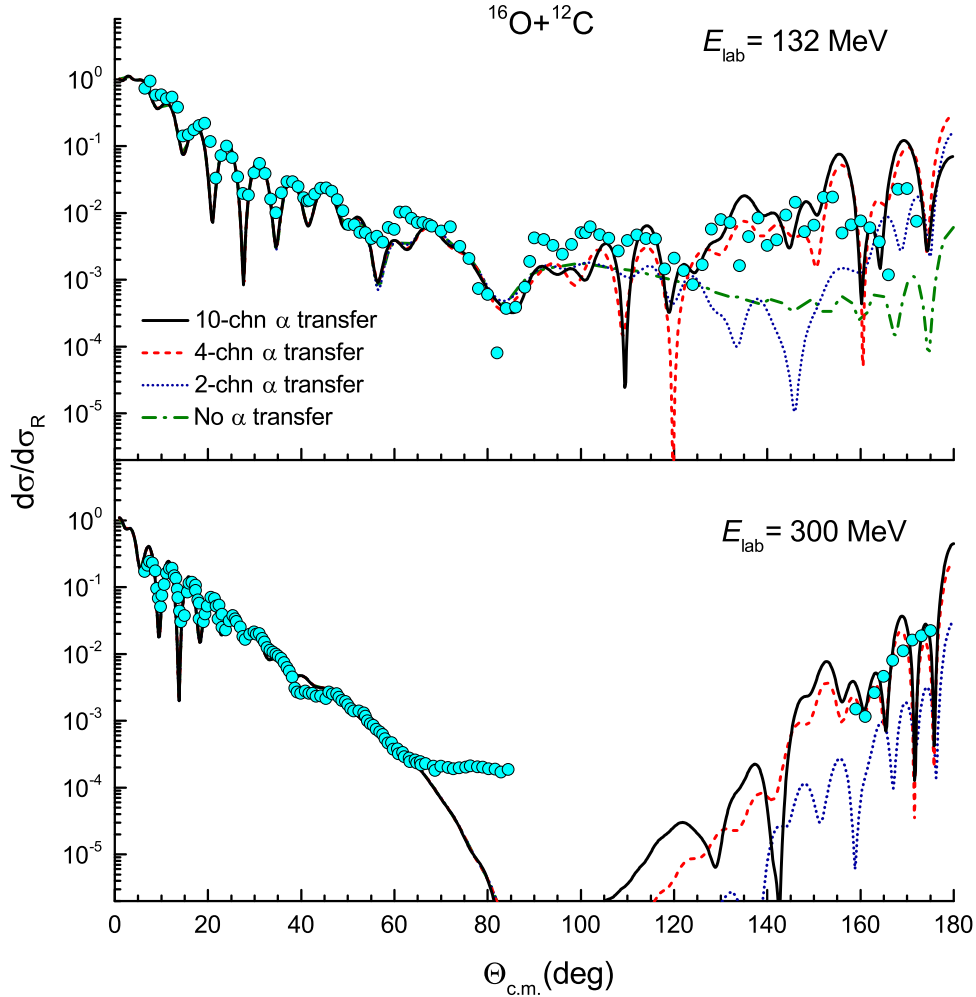
21

FIG. 8. The same as Fig. 7 but for the elastic $^{16}$O+$^{12}$C scattering data measured at $E_{\mathrm{lab}} = 132$ MeV [9, 10], and 300 MeV [12].

scattering cross section falls exponentially with the increasing angles, and cannot be seen at all in the backward region. The present CC results thus show that the scenario suggested by Ohkubo and Hirabayashi [25] for the large-angle oscillation of the elastic $^{16}$O+$^{12}$C cross section observed at $E_{\mathrm{lab}} = 115.9$ MeV is not realistic. In fact, the CC calculation taking into account the couplings to the low-lying excitations of $^{16}$O and the $^{12}$C core cannot give rise to some "reflective" wave that interferes with the elastic scattering wave at backward angles. As discussed above in Sect. II, it is not the CC effect but the use of a very small diffuseness of the WS imaginary potential in Ref. [25] that boosts the near-side scattering wave at backward angles for the interference with the far-side scattering wave, leading to the enhanced oscillation of the elastic cross section (as illustrated in Fig. 3).

TABLE V. The best-fit OP parameters (1) used in the 10-channel CRC analysis of the elastic $^{16}$O+$^{12}$C scattering at $E_{\text{lab}} = 100 - 300$ MeV that includes both the direct and indirect $\alpha$ transfers. All quantities are the same as those presented in Table I.

| $E_{\text{lab}}$ (MeV) | $N_R$ | $J_R$ (MeV fm$^3$) | $W_V$ (MeV) | $R_V$ (fm) | $a_V$ (fm) | $J_W$ (MeV fm$^3$) | $\sigma_R$ (mb) |
|---|---|---|---|---|---|---|---|
| 100 | 0.930 | 310.1 | 5.59 | 6.01 | 0.40 | 27.6 | 1331 |
| 115.9 | 0.910 | 301.6 | 5.50 | 6.00 | 0.40 | 27.1 | 1332 |
| 124 | 0.920 | 304.0 | 6.00 | 5.86 | 0.46 | 28.0 | 1347 |
| 132 | 0.945 | 311.3 | 7.60 | 5.99 | 0.55 | 38.5 | 1436 |
| 300 | 0.912 | 281.7 | 17.70 | 5.60 | 0.68 | 77.5 | 1551 |

With the direct and indirect $\alpha$ transfers taken into account, the elastic $^{16}$O+$^{12}$C cross section is indeed enhanced at large angles. From the CRC results shown in Figs. 7 and 8 one can see that the indirect $\alpha$ transfer is vital for a proper description of the enhanced oscillation of the elastic $^{16}$O+$^{12}$C cross section at backward angles. Our CRC results also show that the indirect $\alpha$ transfer through the $2_1^+$ excitation of the $^{12}$C core is the dominant transfer channel (see, in particular, the CRC results for the elastic $^{16}$O+$^{12}$C scattering at $E_{\text{lab}} = 300$ MeV). This is naturally explained by the large $S_\alpha$ value predicted for the $\alpha+^{12}$C$_{2_1^+}$ configuration in the dissociation of $^{16}$O (see Table IV). The coupling effects to the $\alpha$ transfer by the $0_2^+$, $3_1^-$, and $2_1^+$ excitations of $^{16}$O are relatively weak and can only be slightly seen in the 300 MeV cross section. The 300 MeV data points at the most backward angles should be a good reference for gauging the strength of the $\alpha$ spectroscopic factor and probing the impact by the $\alpha$ transfer on the elastic $^{16}$O+$^{12}$C scattering. Like the results obtained earlier by Rudchik *et al.* [24], the use of the small $\alpha$ spectroscopic factors given by the traditional (old) definition of $S_\alpha$ in our CRC calculation gives a much smaller elastic $\alpha$ transfer cross section cross section at backward angles, leaving the large-angle elastic $^{16}$O+$^{12}$C data unexplained at the considered energies. Therefore, the present CRC results for the elastic $^{16}$O+$^{12}$C scattering seems to support the use of the *new* definition of the $\alpha$ spectroscopic factor [29, 42]. In this connection, more theoretical and experimental studies of the $\alpha$ transfer and knock-out reactions are highly desired for the systematic and reliable information on the spectroscopic
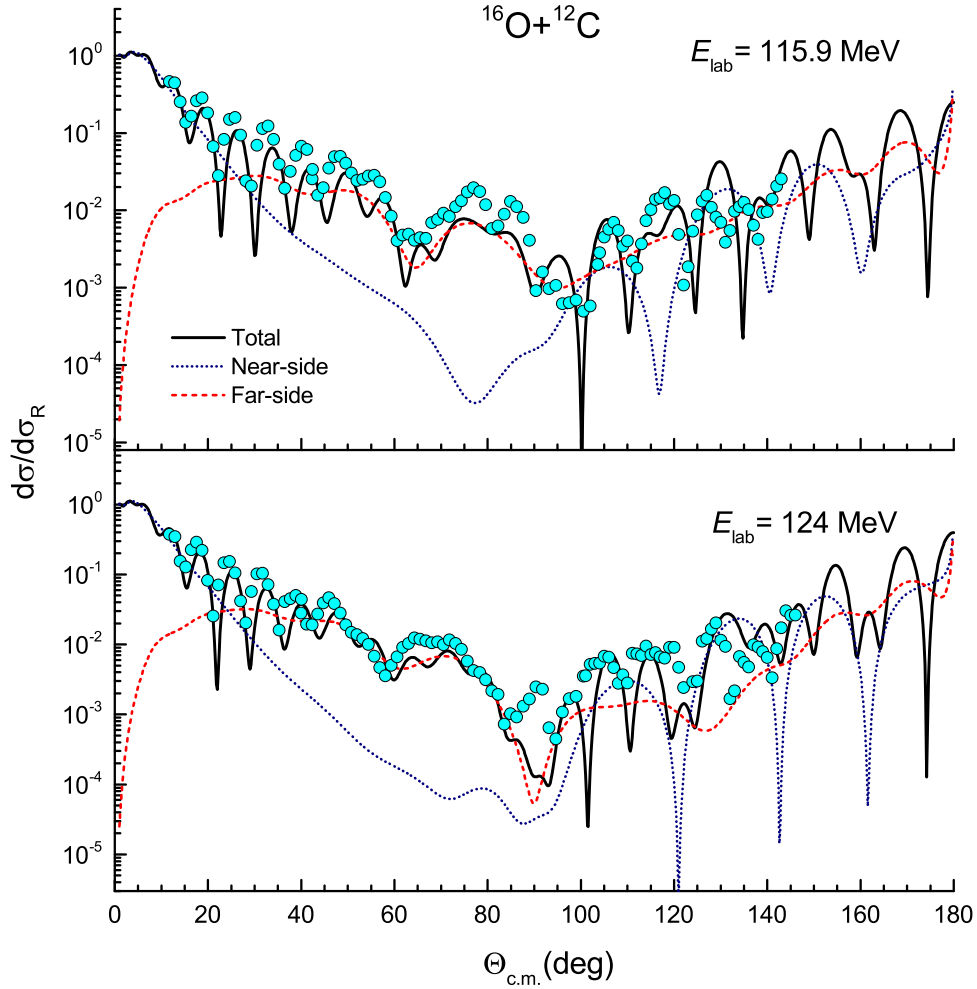
FIG. 9. 10-channel CRC description (solid lines) of the elastic $^{16}O+^{12}C$ data measured at $E_{lab} = $ 115.9 and 124 MeV [11]. The total elastic $^{16}O+^{12}C$ cross section is decomposed into the near-side (dotted lines) and far-side (dashed lines) contributions (2) using Fuller's method [36].

properties of the $\alpha$-cluster dissociation of light nuclei.

As discussed above in Sect. II, the enhanced oscillation of the elastic $^{16}O+^{12}C$ cross section observed at backward angles could be reproduced in the conventional OM calculation only if a very small diffuseness of the WS imaginary OP is used. Such an unusual WS imaginary OP enhances the near-side scattering at large angles, and gives rise, therefore, to a strong near-far interference there. In general, the near-side component of the elastic nucleus-nucleus scattering is dominant in the surface region, at forward angles only. The large-angle scattering (if not suppressed by the strong absorption) is refractive and mainly of the far-side strength [3, 37, 38]. Therefore, a scenario for the strong near-side surface

scattering at backward angles is very unlikely. Given the strong impact of the $\alpha$ transfer on the elastic $^{16}$O+$^{12}$C scattering at large angles shown in Figs. 7 and 8, it is of interest to explore whether the $\alpha$ transfer process also enhances the near-side scattering at backward angles. For this purpose, the total elastic amplitude $f(\theta)$ given by the full (10-channel) CRC calculation has been decomposed into the near-side and far-side components (2) using the Fuller's method [36], and the results are shown in Fig. 9. One can see that the elastic $\alpha$ transfer indeed enhances the strength of the near-side scattering at backward angles and, in the same way as shown in the OM results in Fig. 3, the near-far interference does give rise to the enhanced oscillation of the elastic $^{16}$O+$^{12}$C cross section at backward angles. However, the enhanced near-side cross section at large angles shown in Fig. 9 is *not* of the true elastic scattering but caused by the elastic $\alpha$ transfer that occurs mainly at the surface, at forward angles. The simple reason why it shows up in the elastic cross section at backward angles is that the $\alpha$ transfer amplitudes at $(\pi - \theta)$ were added to the elastic scattering amplitude at $\theta$, using the relation (7). Therefore, the enhanced near-side cross section at large angles shown in Fig. 9 is not an artificial effect caused by a specific numerical technique of the OM calculation, but originates naturally from the $\alpha$ transfer process. The CRC results were obtained using the $^{16}$O+$^{12}$C real folded potential and WS imaginary potential with a normal diffuseness $a_V \approx 0.4 - 0.6$ fm (see Table V). We conclude, therefore, that the unusual imaginary WS potential having a very small diffuseness deduced from the original OM analysis of these data [11] probably mimics the dynamic polarization of the OP by a strong coupling between the true elastic $^{16}$O+$^{12}$C scattering channel and different $\alpha$ transfer channels.

## IV.   IMPACT BY OTHER TRANSFER CHANNELS

It was shown in Ref. [24] that the two-step transfer processes such as the nucleon transfer or sequential transfers of a neutron (proton) and $^3$He (triton) also contribute to the enhanced backward-angle oscillation of the elastic $^{16}$O+$^{12}$C cross section at low energies. Therefore, it is also of interest for the present research to investigate explicitly the contribution from such transfer processes, to see if they can alter the important conclusion made above on the impact by $\alpha$ transfer.

In the CRC analysis of the mentioned transfer channels, the real optical potentials for

all the outgoing channels were calculated in the DFM using the g.s. densities of $^{11}$B, $^{11,13}$C, $^{13,15}$N, $^{15,17}$O, and $^{17}$F given by the independent particle model (IPM) [60]. The same WS imaginary OP was assumed for the entrance and exit channels, with the parameters given in Table I for each energy. The nucleon- and ($A = 3$) cluster binding potentials were chosen in the WS form with the fixed radius $r_0 = 1.25$ fm and diffuseness $a = 0.65$ fm, while the WS depths were adjusted to reproduce the observed nucleon- and ($A = 3$) cluster separation energies. The nucleon spectroscopic factors were taken from the compilation by Tsang *et al.* [61] which is based on a systematic DWBA analysis of $(d, p)$ reactions, and also in a good agreement with the SM results. For simplicity, the isospin symmetry was adopted for the neutron and proton spectroscopic factors. Due to the lack of the experimental data for $^3$He and triton spectroscopic factors, we have used the values predicted by the SM as quoted in Ref. [24].

### A. Nucleon transfer reaction

The strength of the coupled channel contribution from the nucleon transfer reactions to the elastic $^{16}$O+$^{12}$C cross section can be determined from the CRC calculation based on the coupling scheme shown in Fig. 10. It is important to note that the two-step (back and forth) nucleon transfer proceeds through the two-way couplings between the initial partition (a) and 4 corresponding nucleon-exchanged partitions shown in Fig. 10, and the CRC equations similar to Eqs. (3)-(4) are solved by an iterative procedure [28, 39]. The total elastic scattering amplitude is then calculated from the *converged* CRC wave function of the elastic scattering channel. It is obvious from Fig. 10 that the $\alpha$-exchanged partition (b) of the $^{16}$O+$^{12}$C system cannot be populated by the nucleon transfer reactions.

One can see from the CRC results shown in Fig. 11 that the neutron and proton transfer channels have a minor coupled channel effect on the elastic $^{16}$O+$^{12}$C scattering cross section at the low energy of 115.9 MeV, and is completely negligible at the higher energy of 300 MeV. Moreover, the nucleon transfer channels do not contribute at all to the formation of the oscillatory pattern of the elastic cross section at large angles. Because the $\alpha$-exchanged partition (b) of the $^{16}$O+$^{12}$C system cannot be populated by the nucleon transfer as shown in Fig.10, the two-step (back and forth) nucleon transfer contributes to the elastic scattering cross section only through the small change of this cross section induced by the coupled
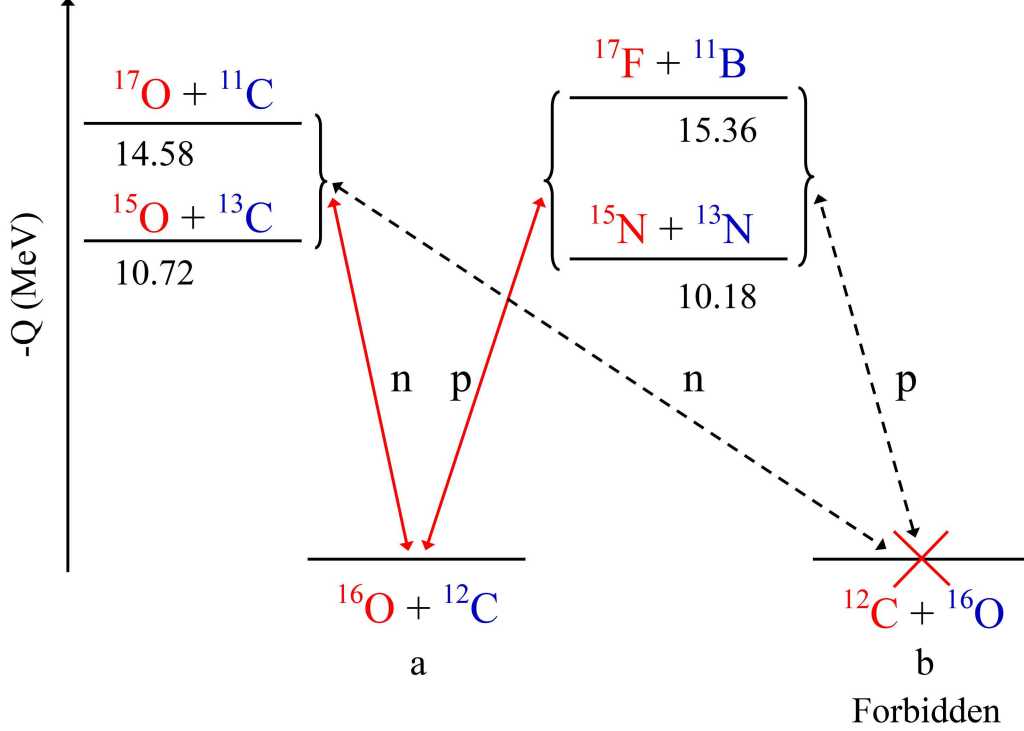
FIG. 10. Explicit coupling between the true elastic scattering and nucleon transfer channels taken into account in the CRC calculation of the elastic $^{16}$O+$^{12}$C scattering. The $\alpha$-exchanged partition (b) of the $^{16}$O+$^{12}$C system cannot be populated by the nucleon transfer reaction.

channels effect (shown in the upper panel of Fig.11). The CRC calculation does not generate separately the elastic two-step nucleon transfer cross sections, denoted in Ref. [24] as $\langle n, n \rangle$ and $\langle p, p \rangle$, that can be added to the elastic scattering cross section. In fact, only if one includes the *forbidden* two-step nucleon transfer to the $\alpha$-exchanged partition (b) of the $^{16}$O+$^{12}$C system, then there appear 4 more CRC equations that lead separately to the two-step $\langle n, n \rangle$ and $\langle p, p \rangle$ transfer cross sections as discussed in Ref. [24]. As a test, we did such a CRC calculation and obtained about the same $\langle n, n \rangle$ and $\langle p, p \rangle$ cross sections as those shown in the right panel of Fig. 7 of Ref. [24], which are still nearly 2 orders of magnitude smaller than the elastic scattering cross section at medium and backward angles. We conclude, therefore, that the nucleon transfer process cannot be the source of the enhanced oscillation of the elastic $^{16}$O+$^{12}$C cross section at large angles.
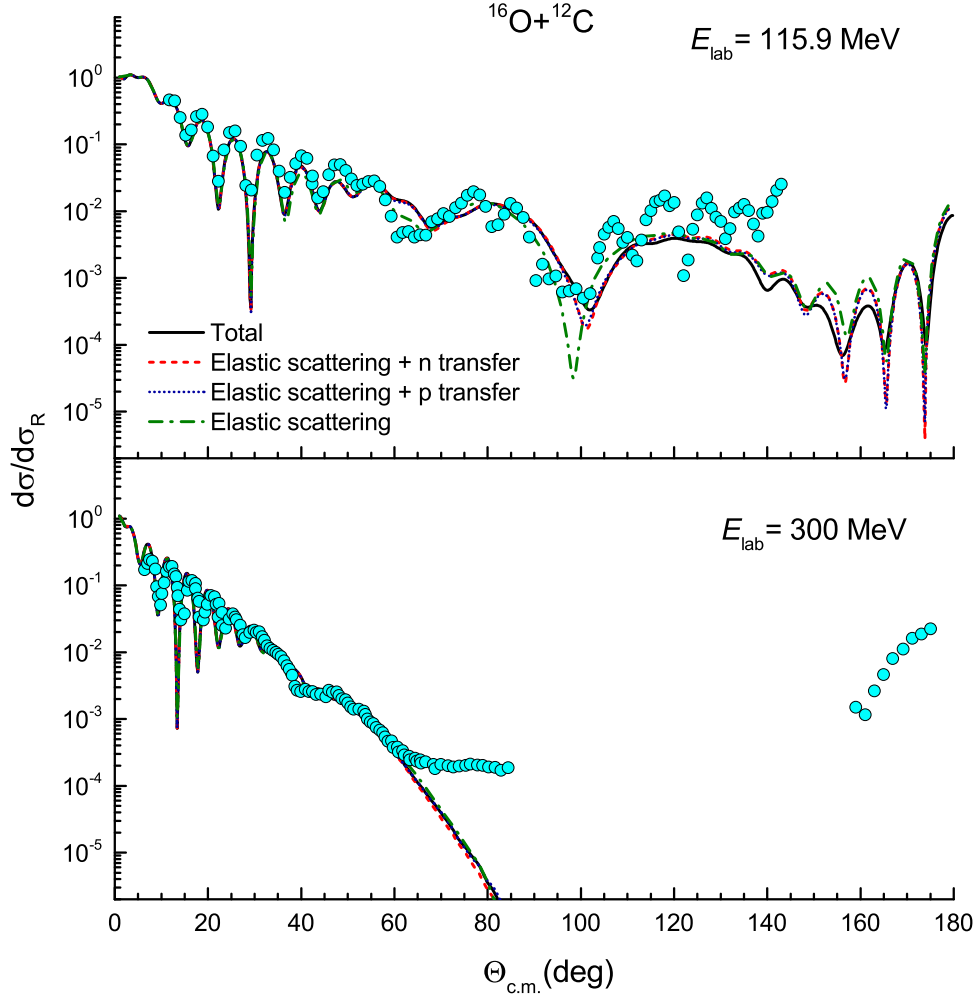
FIG. 11. CRC description of the elastic $^{16}O+^{12}C$ scattering data measured at $E_{lab} = 115.9$ [11] and 300 MeV [12] based on the coupling scheme shown in Fig. 10. The solid lines are the results given by the full coupling between the true elastic scattering and all nucleon transfer channels. The CRC results obtained separately with the coupling to the neutron- or proton transfer channel are shown as the dashed and dotted lines, respectively. The dash-dotted lines are the results of the OM calculation alone.

## B. Sequential transfers of the neutron-$^3$He and proton-triton pairs

Another possible source for the backward-angle enhancement of the elastic $^{16}O+^{12}C$ cross section is the sequential two-step transfer of the neutron-$^3$He or proton-triton pair [24] that naturally populates the $\alpha$-exchanged partition (b) of the $^{16}O+^{12}C$ system via the two-way coupling scheme shown, e.g., for the $\langle n,^3$He$\rangle$ transfer in Fig. 12.

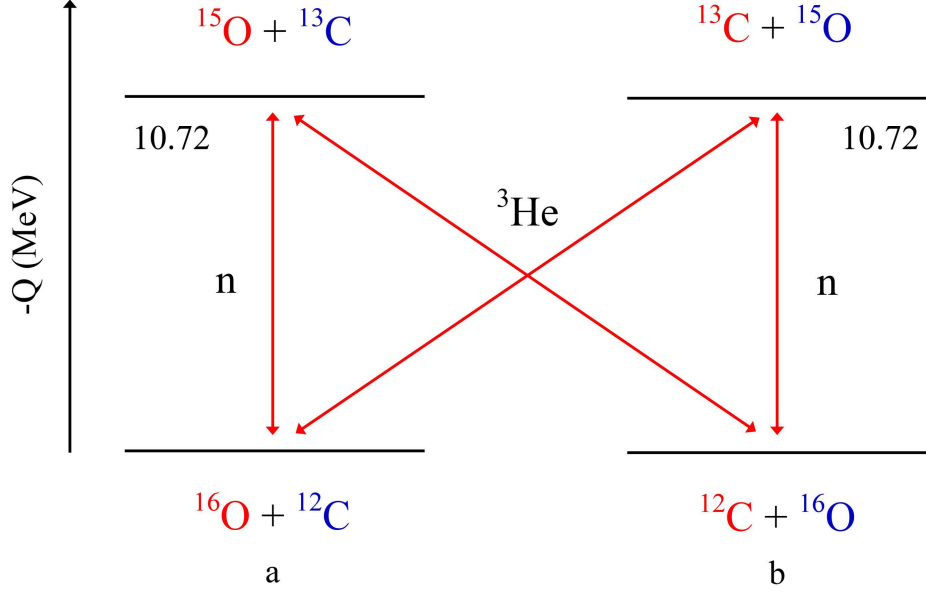The results of the CRC calculation based on the coupling scheme illustrated in Fig. 12 are

28

FIG. 12. Two-way coupling between the true elastic scattering and sequential $\langle n, {}^3\text{He}\rangle$ transfer channels taken into account in the CRC calculation of the elastic $^{16}\text{O}+^{12}\text{C}$ scattering. The coupling scheme for the sequential $\langle p, {}^3\text{H}\rangle$ transfer via the $^{15}\text{N}+^{13}\text{N}$ partitions at $-Q = 10.18$ MeV is exactly the same.

shown in Fig. 13. One can see that the sequential two-step transfers of the $n-^3\text{He}$ and $p-^3\text{H}$ pairs do have some impact on the elastic $^{16}\text{O}+^{12}\text{C}$ cross section at backward angles. At the low energy of 115.9 MeV, these transfer processes have only a minor effect on the backward-angle oscillation, while at 300 MeV they give rise to an enhanced oscillation of the elastic cross section at backward angles, but the calculated cross section still underestimates the data by about two orders of magnitude. These results of our CRC analysis of the sequential two-step $\langle n, {}^3\text{He}\rangle$ and $\langle p, {}^3\text{H}\rangle$ transfers to the $\alpha$-exchanged partition (b) show clearly that they cannot contribute significantly to the observed oscillation of the elastic $^{16}\text{O}+^{12}\text{C}$ cross section at backward angles. Such effect is clearly due to the direct and indirect $\alpha$ transfer processes discussed in Sect. III C.

**SUMMARY**

The enhanced backward-angle oscillation of the elastic $^{16}\text{O}+^{12}\text{C}$ scattering cross section observed at low energies was shown to distort strongly the smooth pattern of the refractive (rainbow) scattering established for this system. To explore this effect, we have performed
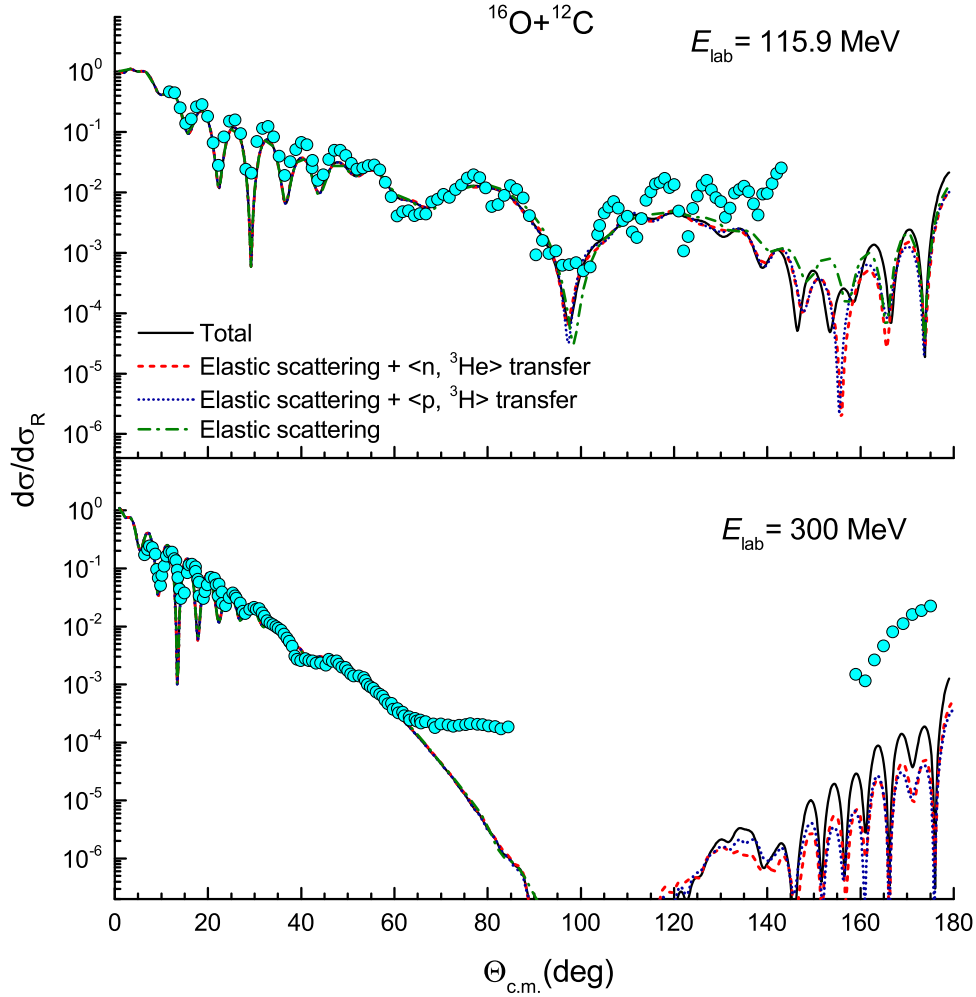
FIG. 13. CRC description of the elastic $^{16}$O+$^{12}$C scattering data measured at $E_{\text{lab}} = 115.9$ [11] and 300 MeV [12] based on the coupling scheme shown in Fig. 12. The solid lines are the results given by the full coupling between the true elastic scattering and sequential two-step $\langle n,^3\text{He}\rangle$ and $\langle p,^3\text{H}\rangle$ transfer channels. The CRC results obtained separately with the coupling to the $\langle n,^3\text{He}\rangle$ or $\langle p,^3\text{H}\rangle$ transfer channel are shown as the dashed and dotted lines, respectively. The dash-dotted lines are the results of the OM calculation alone.

a detailed CRC analysis of the elastic $^{16}$O+$^{12}$C scattering, taking explicitly into account the coupling between the elastic scattering and different $\alpha$ transfer channels, using the folded $^{16}$O+$^{12}$C and $^{12}$C+$^{12}$C potentials as the real optical potentials for these systems. The direct (elastic) $\alpha$ transfer alone was found to account properly for the enhanced oscillation of the elastic cross section at backward angles only by using a best-fit $\alpha$ spectroscopic factor that is much larger than the $S_\alpha$ values predicted by different structure models.

The disagreement of the best-fit $S_\alpha$ deduced from the CRC analysis of the direct $\alpha$ transfer and those predicted by the structure calculations lead us to consider the indirect $\alpha$ transfer channels. With the elastic scattering channel coherently coupled to the inelastic scattering channels as well as to the direct and indirect (via the low-lying excitations of $^{16}$O and the $^{12}$C core) $\alpha$ transfer channels in the present CRC calculation, a satisfactory description of the considered elastic $^{16}$O+$^{12}$C data has been achieved, using the $\alpha$ spectroscopic factors predicted by the large scale SM calculation (the cluster-nucleon configuration interaction model by Volya and Tchuvilsky [29, 31]). The indirect $\alpha$ transfer via the $2_1^+$ excitation of the $^{12}$C core was found to be the dominant $\alpha$ transfer channel. Thus, our CRC results seem to support, for the first time in the direct reaction studies, the use of the *new* microscopic definition of the $\alpha$ spectroscopic factor [29, 42].

The decomposition of the total elastic amplitude into the near-side and far-side components using the Fuller's method [36] allowed us to conclude that the enhanced backward-angle oscillation of the elastic $^{16}$O+$^{12}$C cross section observed at low energies is caused by the interference between the near-side and far-side scattering waves. While the far-side scattering wave is of the true elastic $^{16}$O+$^{12}$C scattering, the unusually strong near-side scattering wave at backward angles is caused by the $\alpha$ transfer, and shows up in the elastic cross section because of the identity of the initial and $\alpha$-exchanged partitions.

For the completeness of the present study, the coupled channel effects to the elastic $^{16}$O+$^{12}$C scattering at low energies from other two-step transfer channels, like the nucleon transfer and sequential transfers of a neutron-$^3$He and proton-triton pairs, were investigated in detail and their contribution to the elastic $^{16}$O+$^{12}$C cross section at backward angles were found negligible. The enhanced backward-angle oscillation of the elastic $^{16}$O+$^{12}$C cross section at low energies is, therefore, mainly due to direct and indirect $\alpha$ transfer processes

The strong coupling effect by the $\alpha$ transfer channels found in the present work is the motivation for a consistent CRC study of the $\alpha$ transfer in both the elastic and inelastic $^{16}$O+$^{12}$C scattering at low energies, which is planned as the follow-up research.

**ACKNOWLEDGMENTS**

[1] G.R. Satchler and W.G. Love, Phys. Rep. **55**, 183 (1979).

[2] M.E. Brandan and G.R. Satchler, Phys. Rep. **285**, 143 (1997).

[3] D.T. Khoa, W. von Oertzen, H.G. Bohlen, and S. Ohkubo, J. Phys. G **34**, R111 (2007).

[4] D.T. Khoa, N.H. Phuc, D.T. Loan, and B.M. Loc, Phys. Rev. C **94**, 034612 (2016).

[5] M.E. Brandan and G.R. Satchler, Phys. Lett. B **256**, 311 (1991).

[6] P. Roussel, N. Alamanos, F. Auger, J. Barrette, B. Berthier, B. Fernandez, L. Papineau, H. Doubre, and W. Mittig, Phys. Rev. Lett. **54**, 1779 (1985).

[7] M.E. Brandan, A. Menchaca-Rocha, M. Buenerd, J. Chauvin, P. De Saintignon, G. Duhamel, D. Lebrum, P. Martin, G. Perrin, and J.Y. Hostachy, Phys. Rev. C **34**, 1484 (1986).

[8] A.C.C. Villari, A. Lépine-Szily, R.L. Filho, O.P. Filho, M.M. Obuti, J.M. Oliveira Jr, and N. Added, Nucl. Phys. A **501**, 605 (1989).

[9] A.A. Ogloblin, D.T. Khoa, Y. Kondō, Yu.A. Glukhov, A.S. Demyanova, M.V. Rozhkov, G.R. Satchler, and S.A. Goncharov, Phys. Rev. C **57**, 1797 (1998).

[10] A.A. Ogloblin, Yu.A. Glukhov, W.H. Trzaska, A.S. Demyanova, S.A. Goncharov, R. Julin, S.V. Klebnikov, M. Mutterer, M.V. Rozhkov, V.P. Rudakov, G.P. Tiorin, D.T. Khoa, and G.R. Satchler, Phys. Rev. C **62**, 044601 (2000).

[11] M.P. Nicoli, F. Haas, R.M. Freeman, S. Szilner, Z. Basrak, A. Morsad, G.R. Satchler, and M. E. Brandan, Phys. Rev. C **61**, 034609 (2000).

[12] M.E. Brandan, A. Menchaca-Rocha, L. Trache, H.L. Clark, A. Azhari, C. A. Gagliardi, Y.-W. Lui, R. E. Tribble, R. L. Varner, J. R. Beene, and G. R. Satchler, Nucl. Phys. A **688**, 659 (2001).

[13] D.T. Khoa, W. von Oertzen, and H.G. Bohlen, Phys. Rev. C **49**, 1652 (1994).

[14] D.T. Khoa, G.R. Satchler, and W. von Oertzen, Phys. Rev. C **56**, 954 (1997).

[15] M.E. Brandan and G.R. Satchler, Nucl. Phys. A **487**, 477 (1988).

[16] D.T. Khoa, W. von Oertzen, H.G. Bohlen, and F. Nuoffer, Nucl. Phys. A **672**, 387 (2000).

[17] F. Michel, G. Reidemeister, and S. Ohkubo, Phys. Rev. C **63**, 034620 (2001).

[18] S. Ohkubo and Y. Hirabayashi, Phys. Rev. C **89**, 051601(R) (2014).

[19] P. Braun-Munziger and J. Barette, Phys. Rep. **87**, 209 (1982).

[20] W. von Oertzen and H.G. Bohlen, Phys. Rep. **19 C**, 1 (1975).

[21] S. Szilner, W. von Oertzen, Z. Basrak, F. Haas, and M. Milin, Eur. Phys. J. A **13**, 273 (2002).

[22] M.C. Morais and R. Lichtenthäler, Nucl. Phys. A **857**, 1 (2011).

[23] Sh. Hamada, N. Burtebayev, K.A. Gridnev, and N. Amangeldi, Nucl. Phys. A **859**, 29 (2011).

[24] A.T. Rudchik *et al.*, Eur. Phys. J. A **44**, 221 (2010).

[25] S. Ohkubo and Y. Hirabayashi, Phys. Rev. C **89**, 061601(R) (2014).

[26] M. Ichimura, A. Arima, E.C. Halbert, and T. Terasawa, Nucl. Phys. A **204**, 225 (1973).

[27] G.R. Satchler, *Direct Nuclear Reactions* (Clarendon, Oxford, 1983).

[28] I.J. Thompson and F.M. Nunes, *Nuclear Reactions for Astrophysics* (Cambridge University Press, Cambridge, UK, 2009).

[29] A. Volya and Y.M. Tchuvilsky, Phys. Rev. C **91**, 044319 (2015).

[30] T. Yamada, Y. Funaki, T. Myo, H. Horiuchi, K. Ikeda, G. Röpke, P. Schuck, and A. Tohsaki, Phys. Rev. C **85**, 034315 (2012).

[31] A. Volya, private communication (unpublished).

[32] D.T. Khoa and G.R. Satchler, Nucl. Phys. A **668**, 3 (2000).

[33] J.E. Poling, E. Norbeck, and R.R. Carlson, Phys. Rev. C **13**, 648 (1976).

[34] D.T. Khoa, Phys. Rev. C **63**, 034007 (2001).

[35] J. Raynal, *Computing as a Language of Physics* (IAEA, Vienna, 1972) p. 75; J. Raynal, coupled-channel code ECIS97 (unpublished).

[36] R.C. Fuller, Phys. Rev. C **12**, 1561 (1975).

[37] M.E. Brandan, M.S. Hussein, K.W. McVoy, and G.R. Satchler, *Comments on nuclear and particle physics*, Vol. 22 (Gordon and Breach, New York, 1996), p. 77.

[38] W.E. Frahn, *Treaties on Heavy-Ion Science* vol. 1, p. 135, ed. D.A. Bromley (Plenum Press, New York, 1984).

[39] I.J. Thompson, Comput. Phys. Rep. **7**, 167 (1988); http://www.fresco.org.uk.

[40] D.T. Khoa and D.C. Cuong, Phys. Lett. B **660**, 331 (2008).

[41] D.R. Tilley, H.R. Weller, and C.M. Cheves, Nucl. Phys. A **564**, 1 (1993).

[42] K. Kravvaris and A. Volya, Phys. Rev. Lett. **119**, 062501 (2017).

[43] T. Fliessbach and H.J. Mang, Nucl. Phys. A **263**, 75 (1976).

[44] T. Fliessbach and P. Manakos, J. Phys. G **3**, 643 (1977).

[45] R.G. Lovas, R.J. Liotta, A. Insolia, K. Varga, and D.S. Delion, Phys. Rep. **294**, 265 (1998).

[46] R. Id Betan and W. Nazarewicz, Phys. Rev. C **86**, 034338 (2012).

[47] R.G. Lovas, Z. Phys. A **322**, 589 (1985).

[48] K.A. Gridnev, N.A. Maltsev, and N.V. Leshakova, Bull. Russ. Acad. Sci. Phys. **77**, 852 (2013).

[49] Sh. Hamada, N. Burtebayev, and N. Amangeldi, Int. J. Mod. Phys. E **23**, 1450061 (2014).

[50] Y. Kanada-En'yo, Phys. Rev. C **96**, 034306 (2017).

[51] S. Okabe, *Tours Symposium on Nuclear Physics II*, edited by H. Utsunomiya *et al.* (World Scientific, Singapore, 1995) p. 112, and private communications.

[52] H. Miska, H.D. Gräf, A. Richter, R. Schneider, D. Schüll, E. Spamer, H. Theissen, O. Titze, and Th.Walcher, Phys. Lett. B **58**, 155 (1975).

[53] Y. Suzuki, Prog. Theor. Phys. **55**, 1751 (1976); **56**, 111 (1976).

[54] I. Rotter, Fortschritte der Physik **16**, 195 (1968).

[55] D. Kurath, Phys. Rev. C **7**, 1390 (1973).

[56] G.J. Wozniak, D.P. Stahel, J. Cerny, and N.A. Jelley, Phys. Rev. C **14**, 815 (1976).

[57] W. Oelert, A. Djaloeis, C.Mayer-Böricke, P. Turek, and S. Wiktor, Nucl. Phys. A **306**, 1 (1978).

[58] K. Umeda *et al.*, Nucl. Phys. A **429**, 88 (1984).

[59] M. Kamimura, Nucl. Phys. A **351**, 456 (1981).

[60] G.R. Satchler, Nucl. Phys. A **329**, 233 (1979).

[61] M.B. Tsang, J. Lee, and W.G. Lynch, Phys. Rev. Lett. **95**, 222501 (2005).